# The development of a method for the visualisation of intra-Golgi vesicle trafficking

**Zaina Ibnahaten**

**MSc by Research**

**University of York**

**Biology**

**September 2023**

# Abstract

The Golgi apparatus relies on the retrograde movement of intra-Golgi vesicles to maintain the cisternal locations of resident glycosylation enzymes. Previous studies have ascertained the structures and functions of tethering factors within the Golgi which mediate and control the movement of retrograde intra-Golgi vesicles containing the glycosylation enzymes. However, the specific interactions between the vesicles and target membranes, as well as the vesicle tethering and fusion processes, are still largely unknown. Here I present a method for the identification of the number of fluorescent molecules present in isolated intra-Golgi vesicles with TIRFM, as well as the generation of an intensity/distance from slide graph to quantify a relationship between the recorded fluorescence of a fluorescently tagged glycosylation enzyme with TIRFM and its distance from the slide surface. This data will be useful in future work to examine the transport, tethering and binding of intra-Golgi vesicles in a cell free assay. Furthermore, I attempted to develop a stable cell expressing tagged B4GALT1 and MGAT1 glycosylation enzymes for use in future cell-free experiments, however confocal microscopy revealed that HaloTag-B4GALT1 does not localise to the Golgi apparatus. From the methods described in this project, a cell line successfully expressing tagged glycosylation enzymes could be developed in the future.

*I declare that this thesis is a presentation of original work and I am the sole author. This work has not previously been presented for a degree or other qualification at this University or elsewhere. All sources are acknowledged as references.*

# Contents

# List of Figures

# List of Tables



# List of Equations

# Introduction

The study of the mechanisms driving vesicle targeting and tethering within cells has been a challenging task in scientific research for decades. Intracellular vesicle trafficking is an essential process within eukaryotic cells to support cellular function through the tagging and sorting of nascent proteins. Intra-cellular vesicle pathways critically rely on specific vesicle fusion to their targets, a process which is coordinated by tethering complexes. Previous studies in orthologous genes in budding yeast have identified the structures and functions of some of these tethering complexes, however their specific interactions with vesicles and target membranes are still unknown. The dissection of intracellular vesicle trafficking is vital for the understanding of diseases involving vesicle trafficking dysregulation, as well as the development of drugs and therapies that target the secretory pathway and broadening our understanding of cell biology.

## The Golgi Apparatus

### Introduction

The Golgi is an organelle found in most eukaryotic cells which is responsible for the modification and packaging of newly synthesised proteins and lipids from the endoplasmic reticulum (ER) into vesicles for delivery to other intracellular membranes and secretion out of the cell. First identified by Camillo Golgi in 1898 (Ghosh, 2020), the Golgi is a dynamic structure comprised of five to seven flattened stacked cisternae around 30-40nm thick (Jamieson and Palade, 1967, Klumperman, 2011) (Figure 1). The distinct cisternae of the Golgi contain different sets of glycosyltransferase and glycosidase enzymes which create modifications to their targets known as glycosylation, resulting in more diverse protein structures and aiding in protein folding and function (Li *et al.,* 2019). Glycosylation is the consecutive enzymatic modification of proteins traversing in cisternae through the Golgi stack and is the most common post-translational modification. This leads to the addition of complex glycans covalently attached to specific amino acids on the proteins, as determined by protein structure, secretory protein load, monosaccharide nucleotide availability, and enzyme levels (Yadav *et al.,* 2022, Suga *et al.,* 2018, Fisher *et al.,* 2019a).

The Golgi contains over 200 glycosyltransferase enzymes which need to be distinctly sorted into separate cisternal locations in order to glycosylate the passing protein accurately. Glycosylation of

nascent proteins is a sequential process which requires the addition of specific residues to the growing glycan chain, and the organisation of glycosylation enzymes into specific cisternae allows for the sequential exposure of the protein to the enzymes (Cottam and Ungar, 2012). The Golgi apparatus is an excellent model organelle for the study of intra-cellular vesicles as it is a highly dynamic and easy to label structure with a constant flux of vesicles from the ER and between cisternae (Blackburn *et al.,* 2019).

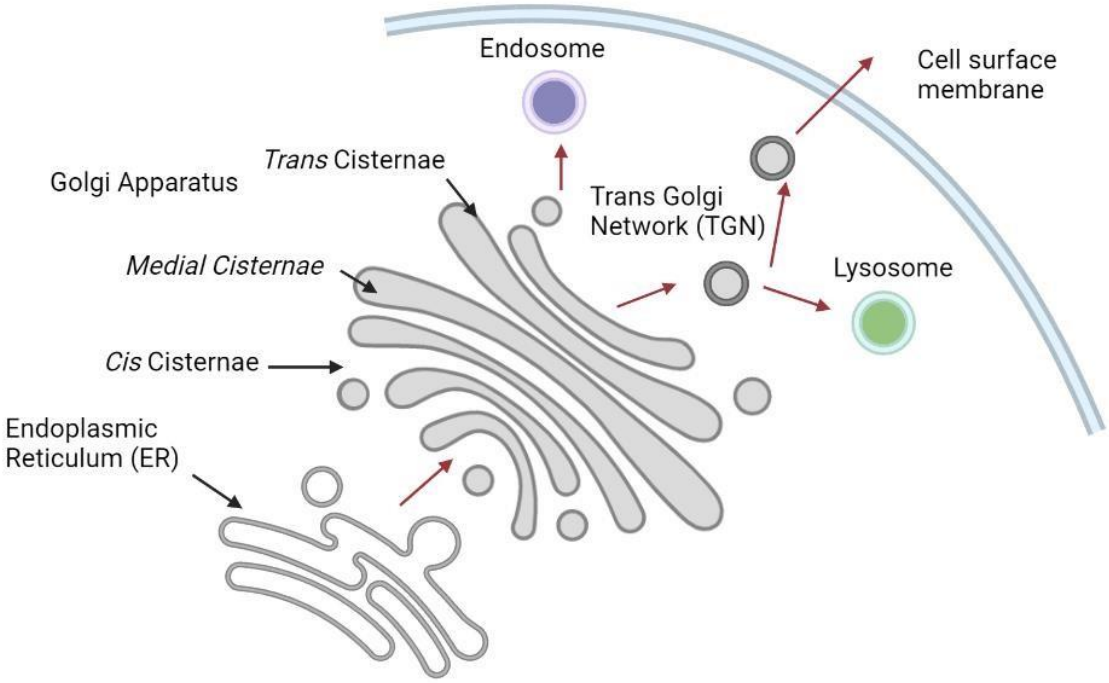


**Figure 1 -** ***Structure and movement of cargo through the Golgi apparatus.*** *Cisternae stacks are formed from vesicles derived from the ER and received by the* cis *cisternae, where cargo is modified, processed and then exported from the trans cisternae and trans-Golgi network to other intracellular membranes such as the endosomes, lysosomes, and plasma membrane for exocytosis. Image adapted from Park et al. (2021).*

## Retrograde Vesicle Movement

The dynamic structure of the Golgi apparatus is due to a constant fusion and fission of retrograde vesicles between the Golgi cisternae in order to facilitate cargo transport. The cisternal maturation model is the most widely accepted method for cargo transport within the Golgi and is described as the maturation of cisternae through the Golgi while maintaining and processing cargo. Exclusive retrograde intra-Golgi COPI (coat protein complex I) vesicle transport sorts the glycosylation enzymes into their active regions of the Golgi (Bonfanti *et al.* 1998). Cargo proteins in vesicles leaving the ER combine with retrograde vesicles containing cis-Golgi enzymes from the medial-Golgi to form a new cis-Golgi. This matures into a medial-Golgi as it progresses into the medial-Golgi stack through the

recycling of cis-Golgi enzymes and receiving of medial-Golgi enzymes. This process is repeated to create the trans-Golgi and trans Golgi network (TGN) as illustrated in Figure 2 (Schmitz *et al.* 2008, Fisher *et al.,* 2019b).

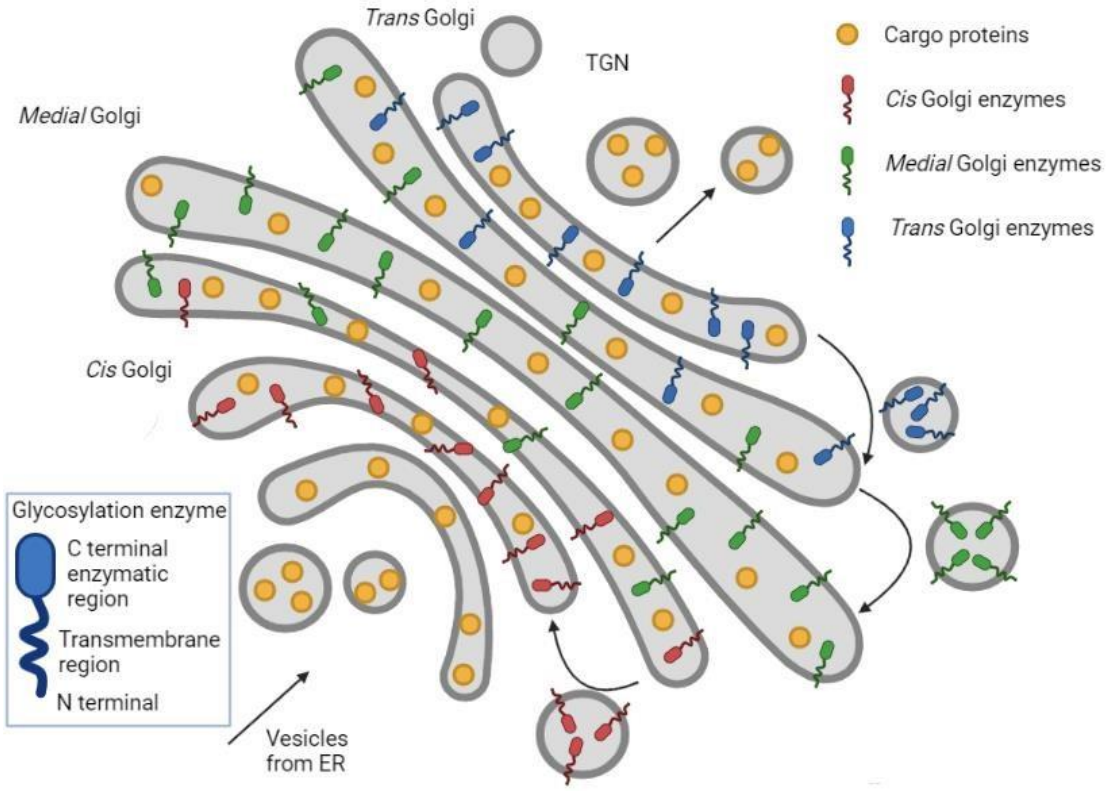


***Figure 2* - Diagram of the cisternal maturation model.** Retrograde vesicle transport retains Golgi enzymes in their regions of the Golgi stack in order to prompt cisternal maturation, along with the generic structure of a glycosylation enzyme.

The cisternal maturation model relies on the specific movement of retrograde vesicles to ensure glycosylation enzymes are sorted into their correct cisterna for their specific function. This specificity is provided by intra-Golgi vesicle targeting and tethering, however the mechanisms for specific retrograde vesicle targeting in the Golgi are not yet well characterised at the molecular level.

## Vesicle Tethering and Fusion

Intra-Golgi vesicle trafficking is a crucial process within the Golgi apparatus to maintain the distinct functions of the cisternae, and is defined as the budding, transport, tethering and fusion of vesicles to cisternae. Vesicle tethering and fusion play crucial roles in determining vesicle target specificity and is orchestrated by a collection of protein interactions which lead to SNARE mediated membrane fusion, allowing for the organisation of glycosylation enzymes within the cisternae of the Golgi (Malsam *et al.,* 2005, Mkhikian *et al.,* 2016). This is exampled through the glycosylation enzymes β-

1,4-Galactosyltransferase (B4GALT1) and alpha-1,3mannosyl-glycoprotein 2-beta-N-acetylglucosaminyltransferase (MGAT1) which are maintained in the trans-Golgi and medial -Golgi respectively, which is accomplished through the regulation of vesicle tethering and fusion.

Initially, membrin (a type of SNARE protein) recruits activated small GTPases from the Arf subfamily to the cisternae surface (Honda *et al.,* 2005, Popoff *et al.,* 2011), which in turn recruits the coat protein COPI which polymerises and deforms the membrane to encase the cargo and form the vesicle (Reinhard *et al.,* 2003, Adolf *et al.,* 2013). The vesicle is then organised by Rab GTPases which recruit further effector proteins including cytoskeletal motors and tethering factors to determine the delivery of the vesicle to its target membrane, one of which is the conserved oligomeric Golgi (COG) complex (Happe and Weidman, 1998).

## The Conserved Oligomeric Golgi Complex

The COG plays a key role in maintaining Golgi homeostasis and coordinating retrograde vesicle tethering in the Golgi. The COG complex is a multi-subunit tethering complex and is highly conserved in every eukaryotic species (Koumandou *et al*., 2007). The current model for how the COG complex facilitates membrane tethering suggests that golgins (coiled-coil tethering factors in the Golgi) on the cisternal surface initiate vesicle contact. They are attached to Rabs on the Golgi surface by their C terminal domain, allowing for the long-range tethering of vesicles through Rab and small GTPase interactions. The golgin head then binds to Rabs on the vesicle membrane surface, which in turn attaches to the COG complex (Figure 3) (Miller *et al.,* 2013, Ungar *et al.,* 2005).

The COG complex can span as far as 80nm with multiple elongated arms to bridge the distance between the membranes, and the different COG subunits interact with the Rabs, golgin and SNAREs to act as a tethering complex to align the two membranes and draw them into close enough proximity to allow for SNARE mediated fusion (Cottam *et al.,* 2014, Willett *et al*., 2013, Miller *et al.,* 2013).

The COG complex interacts with several golgins, Rab type small GTPases, and SNAREs to coordinate retrograde vesicle tethering. Yeast two hybrid assays show multiple Rabs bind to subunits 4, 5 or 6 of COG, while all golgins interact with Cog2 and SNAREs interact with Cog8, suggesting that COG assists multiple protein interactions to mediate vesicle tethering and fusion within the Golgi via specific reaction hubs within its structure (Miller *et al.* 2013). However, this current model of distinct COG subunits mediating specific tethering and fusion proteins is based primarily on interaction data collected in yeast two hybrid assays and Co-Immunoprecipitation assays, and may not reflect in vivo COG functionality, as it is most likely not every single possible interaction is being utilised within the

cell (Willet *et al.* 2013, Laufman *et al.,* 2013). Furthermore, information on the specific sequence of these interactions and their timings, especially in the rapid and dynamic interactions displayed within the Golgi, are currently unknown.

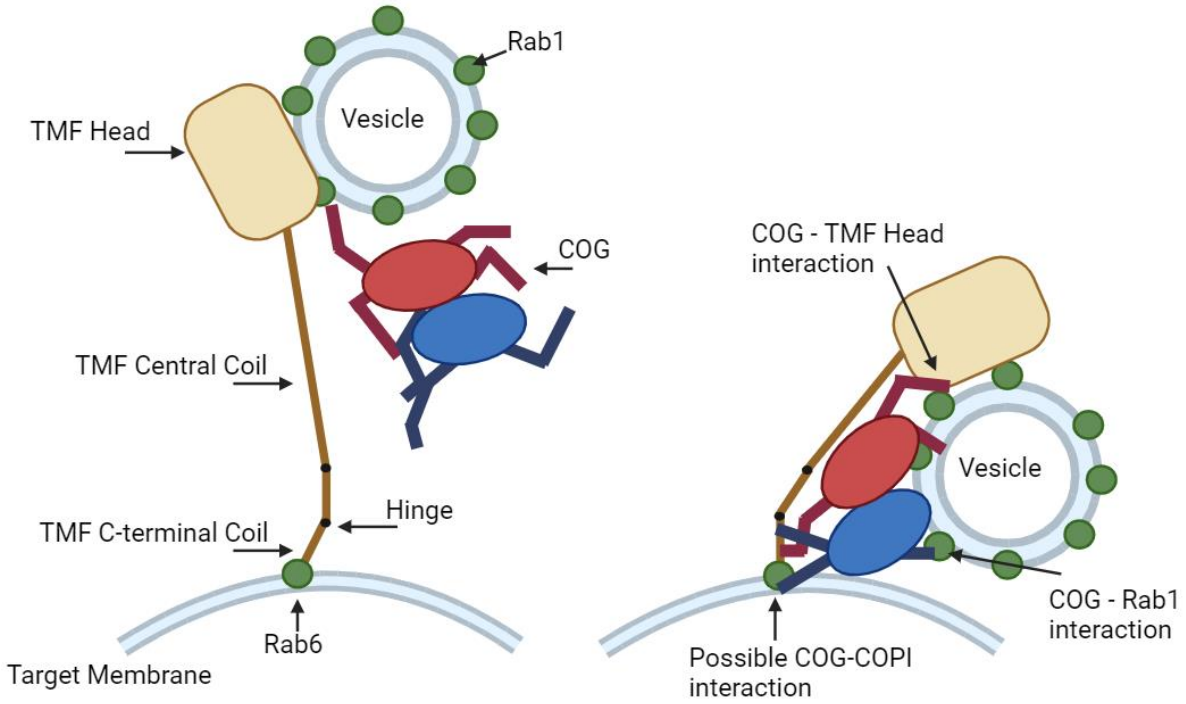


***Figure 3*** **- Model of COG mediated tethering.** The golgin 'TATA element modulatory factor' (TMF) interacts with Rab6 and Rab1 on the cisterna and vesicle, which coupled with COG interactions pulls the vesicle closer to the cisterna, allowing SNARE interactions to initiate membrane fusion. Image adapted from Miller et al. (2012).

Mutations in COG are shown to have many effects within the Golgi and on overall cellular function, including disruption of the cell wall in yeast assays, and altered protein glycosylation (Gremillion *et al.,* 2014). COG truncation mutations lead to destabilisation of other COG subunits, resulting in altered localisation of the glycosylation enzymes, which in turn leads to glycosylation deficiencies (Foulquier *et al.,* 2006). A sub-category of these glycosylation deficiencies can lead to congenital disorders of glycosylation (CDGs), a group of disorders observed in humans which highlight the importance of investigating and understanding intra-Golgi vesicle targeting (Dulary *et al.,* 2017).

## B4GALT1 and MGAT1

For this project, the glycosylation enzymes B4GALT1 and MGAT1 were selected for the investigation into retrograde vesicle transport, to be tagged with HaloTag and SNAPtag respectively. B4GALT1 and MGAT1 are maintained in the trans-Golgi and medial-Golgi respectively, with B4GALT1 transferring galactose onto available GlcNAc molecules, and MGAT1 transferring GlcNAc onto the first mannose branch (Yip *et al.,* 1997, Qasba *et al.,* 2008). These enzymes were selected because they are localised to distinct regions of the Golgi apparatus, meaning that the orientation of the Golgi can be determined, and it can be confirmed that the isolated vesicles locate to their correct respective Golgi cisternae. This opens up future experiments where the effects of inhibiting known trafficking factors can be observed on the localisation of B4GALT1/MGAT1 containing vesicles to their cisternae.

## Vesicle Specificity

Retrograde vesicles in the Golgi containing different cisternae specific cargo have been shown to use different Rabs and members of the golgin family for tethering (Malsam *et al.,* 2005, Willett *et al.,* 2013), suggesting specificity in vesicle tethering plays a role in glycosylation enzyme organisation in the Golgi. 12 of the >60 mammalian Rabs are shown to interact with COG subunits, highlighting the influence of Rabs on vesicle tethering specificity. The switching between active and inactive forms of Rabs allows for control of vesicle tethering, as activated GTP-bound Rabs are available for binding with Golgi tethering molecules (Zerial and McBride, 2001). Furthermore, the specific cargo receptors on the surface of vesicles read the N terminus of the transmembrane glycosylation enzymes, suggest that multiple factors play a role together in determining vesicle specificity (Malsam *et al.,* 2005).

## Total Internal Reflection Fluorescence Microscopy Imaging of Vesicle Transport

### Introduction

The visualisation of vesicle transport through tagged glycosylation enzymes requires a fluorescence microscopy technique with an ability to track the movement and fusion of vesicles containing one or more fluorophore-tagged proteins. Total internal reflection fluorescence microscopy (TIRFM) can provide high-resolution real-time visualisation of single fluorophores in vitro, allowing for the identification of the rapid events of vesicle trafficking, fusion, and cargo delivery. TIRFM was selected for the development of this transport assay as it provides many advantages compared to other light microscopy techniques such as confocal microscopy, including a significantly reduced signal-to-noise ratio with almost no out of focus fluorophores collected due to the optical sectioning afforded by the near-field illumination (Fish, 2015). The excitation of fluorophores by total internal reflection illumination occurs only within a thin optical section, thus enhancing the ability to spatially resolve fluorescently-labelled features in this section and allowing for single fluorophore detection if the fluorophore concentration is very low (Kudalkar *et al.,* 2016, Martin-Fernandez *et al.,* 2013). Furthermore, TIRFM offers the accurate detection of rapid changes in fluorescence intensity, information which can then be correlated into a 3D model of vesicle movement. The benefits of the optical sectioning provided by TIRFM along with its compatibility with cell free assays makes it an ideal method for the tracking of vesicle tethering and fusion in real-time.

TIRFM is based on the principle of total internal reflection, where light travelling through a higher refractive index medium (e.g. glass) is reflected at an interface with a lower refractive index medium (e.g. water), if the angle of incidence is at a sufficiently large angle (known as the critical angle), to generate a near-field phenomenon known as an evanescent wave or field. This evanescent wave decays exponentially from the interface of the two media, penetrating up to 200nm into the sample medium (Kudalkar *et al.,* 2016). The limitation of the depth of the evanescent field allows for only fluorophores close to the slide surface to be sufficiently excited to fluoresce, and fluorophores further from the evanescent wave will not fluoresce, leading to a high signal-to-noise ratio and a significant reduction in background fluorescence. Fluorescent molecules closer to the slide are exposed to a stronger evanescent wave and therefore appear brighter to the collection objective and have a higher recorded intensity (Figure 4), meaning the distance of a fluorophore from the surface of the slide can be inversely correlated with its fluorescent intensity.

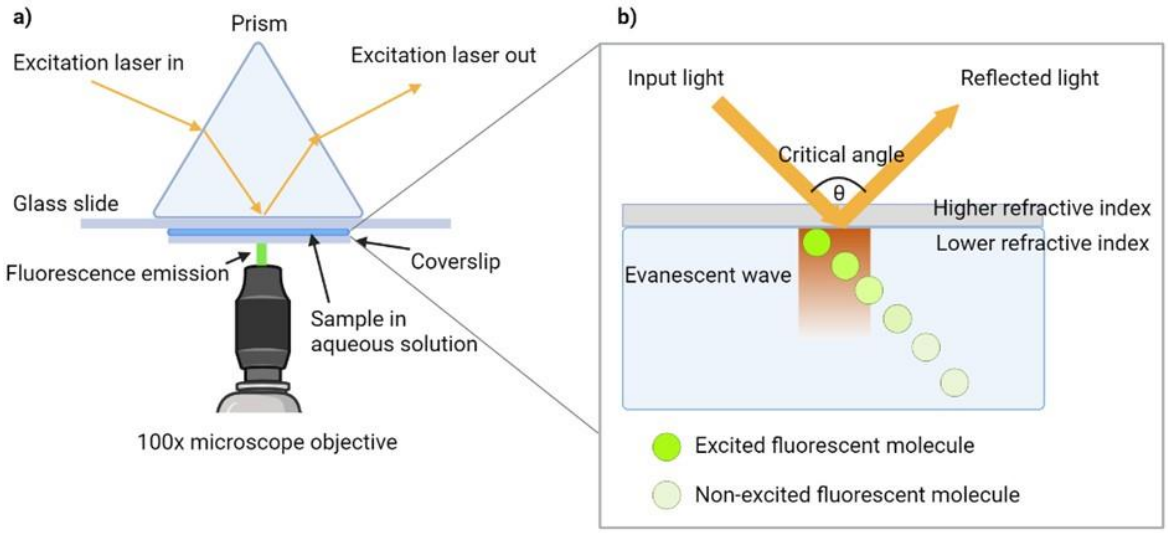


***Figure 4* - Diagram of TIRFM.** (a) Overall movement of light through a prism onto a sample to produce the evanescence wave. (b) Incident excitation light interacts with the glass-water interface at or above a critical angle, causing total internal reflection and the generation of an evanescent wave in solution the intensity of which exponentially decays as it gets further from the glass surface. Fluorophores closer to the glass-water interface are exposed to a more intense evanescent wave and therefore appear brighter to the collection objective and have a higher recorded fluorescence intensity (Fish, 2015).

## Previous Uses of TIRFM

TIRFM has a wide range of applications in imaging, from the study of membrane dynamics to single molecule experiments. Particularly, TIRFM has been utilised in the quantification of vesicle exocytosis (Becherer *et al.,* 2007) and investigation of synaptic vesicles (Aryal *et al.,* 2021).

TIRFM has also been used for investigating multiple parameters of vesicles, including a study by Veit *et al*. (2022) where they developed a method for studying proteoliposomes (artificial vesicles composed of lipids and membrane proteins) using single-vesicle fluorescence bleaching with TIRFM. This study successfully labelled proteoliposomes containing the ATPase AHA2 with Alexa Fluor 647 and visualised them with TIRFM, obtaining their fluorescence intensity over time (s) (Figure 5). This study successfully captured the photobleaching of individual fluorophores, showing the number of AHA2 proteins in each vesicle based on the number of photobleaching steps. This data highlights the quantitative power of TIRFM intensity detection and is a method that can be applied to this project to help determine the number of fluorescent particles in each vesicle.

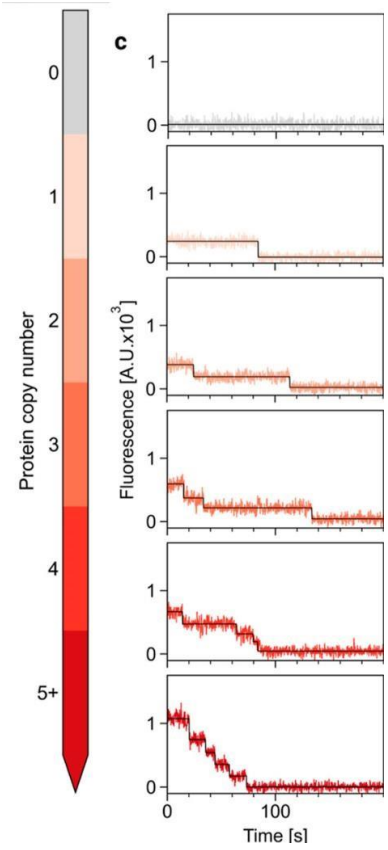


***Figure 5* - Photobleaching traces for proteoliposomes visualised with TIRFM showing separate vesicle categories**. Photobleaching of individual fluorophores highlights number of fluorescently labelled AHA2 proteins in each proteoliposome, as shown in each trace (protein copy number 1-5+). Image adapted from Veit et al., (2022).

Furthermore, the step changes in fluorophore intensity over time can be applied to the visualisation of membrane fusion events. In their study, Nikolaus *et al*. (2021) utilised TIRFM to characterise individual membrane fusion events through the development of a TIRF microscope where the polarisation of the excitation light could be controlled to monitor the docking and fusion of LR-PE fluorescently labelled unilamellar vesicles onto a planar bilayer supported on the coverslip. This study was successful in identifying the optimal polarisation where fluorescence emission was maximal, as well as correlate total intensity of an area of vesicle fusion to the individual stages of vesicle docking and fusion, something that can hopefully be replicated in future research with this project (Figure 6).

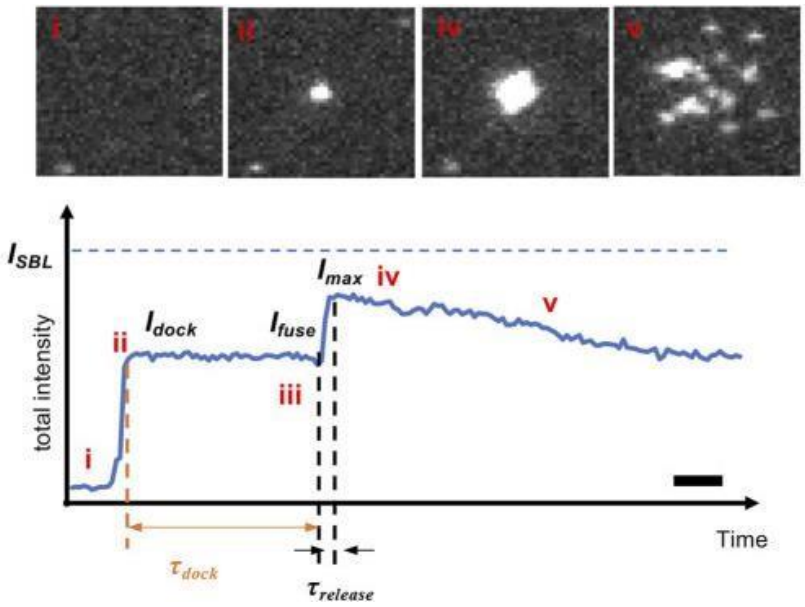


***Figure 6* - Intensity changes during vesicle fusion to a bilayer.** a) TIRFM detected intensity changes during liposome-supported bilayer fusion. LR-PE fluorescently labelled unilamellar vesicles show membrane docking and fusion as intensity increases then disperses (i-v). b) Total intensity of vesicles is shown against time, and an increase in intensity indicates vesicle docking to target membrane as it enters the evanescent field, followed by another increase with fusion as fluorophores move closer to slide surface. This data highlights the effectiveness of this method for the investigation of vesicle trafficking in the Golgi. Image adapted from Nikolaus et al., (2021).

## Limitations of TIRFM

Many TIRFM experiments require the quantification of the evanescent field penetration depth in order to measure the motion in the z-direction (relative to the imaging surface) of the molecules being visualised. In theory, the depth of the evanescent field can be calculated from the known refractive indices of the glass slide and the media the samples are in, along with the incident illumination angle and the wavelength of excitation light (Equation 1). However, in practice the precise depth is considerably less certain due to the incident light comprising of a range of angles and not being perfectly parallel, as well as the optics guiding the excitation light source scattering light which generates multiple propagating light sources, some of which do not exponentially decay from the slide surface (Brunstein *et al.,* 2014). These limitations are something this project aims to address through the development of a fluorescence intensity versus distance from slide surface calibration curve. This will quantify how the intensity of a fluorophore relates to its distance from the surface of the slide and determine the maximum depth within the evanescent field where a fluorophore can be reliably detected.

$$\mathrm{d} = \lambda_0/4\pi\,(\mathrm{n_2}^2\ \sin^2\theta - \mathrm{n_1}^2)^{1/2};$$
$$[\mathrm{alternatively}, \mathrm{d} = \lambda_0/(4\pi\,\mathrm{n_2})$$
$$\times\,((\sin^2\theta/\sin^2\theta_{\mathrm{critical}}) - 1)^{1/2}]$$

***Equation 1 - Equation to calculate the depth of the evanescent field****. The depth of the evanescent field (d) is calculated from the wavelength of excitation light ($\lambda_0$), the refractive index of the glass slide ($n_2$), and the refractive index of the media the vesicles are in ($n_1$). Equation from Fish, (2015).*

## Self-labelling Tags

The self-labelling protein tags HaloTag and SNAPTag are valuable tools in the fluorescent detection of proteins of interest by TIRFM. They will be utilised in this project to tag MGAT1 and B4GALT1. These modified enzyme tags can be cloned onto any protein of interest and covalently link to ligands bound to functional groups rapidly and irreversibly, allowing for the function of the ligand to be changed without needing to re-clone the protein. In this case, membrane permeable fluorescent ligands such as tetramethylrhodamine (TMR), Oregon Green, Coumarin, and 505-Star can be utilised in the staining of tagged glycosylation enzymes to track vesicle movement.

The benefits of these tags include their extreme specificity and high-affinity binding to covalent ligands, their versatility to label a wide range of proteins, and the ability to change their ligands and therefore the colour of the covalently linked fluorophore. The latter attribute is very useful here because vesicles and Golgi cisternae can be labelled in multiple different colours without the need to generate a new cell line (England *et al.,* 2015).

## Nocodazole

Nocodazole is another valuable tool in the analysis and confirmation of the successful addition of the self-labelling tags HaloTag and SNAPTag to the glycosylation enzymes in the Golgi. Nocodazole binds to beta-tubulin within cells, leading to the irreversible destabilisation of microtubule polymerisation (Tie *et al.,* 2022). One key effect of this is the dispersion of the Golgi ribbon into multiple distinct ministacks. Ministacks have previously been shown to be valid representations of the native Golgi, with similar structures and cellular functions (Cole *et al.,* 1996). For this project, the tagged glycosylation enzymes need to be shown to localise to their correct cisternae in the Golgi. This is simplified with Golgi ministacks as they are significantly smaller than the whole Golgi and clear cis-to-

trans polarity can be determined through microscopy, meaning the positions of tagged proteins of interest relative to marker glycosylation enzymes can be identified.

**Cell Free Assays**

Cell free assays are used in research to study the activity of cellular components outside of living cells, allowing for easier manipulation and observation. This is achieved through isolating cellular fractions through ultracentrifugation, then reintroducing the fractions of interest. In this assay, the shallow penetration depth of the TIRFM evanescent field is a limiting factor in the visualisation of the Golgi apparatus due to the relatively large size of the cells, so a cell free assay is required to ensure the Golgi cisternae and vesicles are as close to the slide as possible and visible.

Previous cell free assays have investigated the role of COG in trans-Golgi vesicle tethering through B4GALT1 fluorescent tagging (Cottam et al. 2013), as well as the identification of multiple vital protein interactions in vesicle tethering, for example the interaction between the coiled-coil tether p115 with Rab1 to recruit it to COPII vesicles to initiate membrane fusion (Allan et al., 2000). This project aims to expand on this research to develop a strategy for the identification of the specific mechanisms of vesicle targeting. Isolated Golgi membranes have been shown to retain their transport activity (Balch et al., 1984) and along with the strict localisation of glycosylation enzymes back to their specific cisternae, cell free assays have proven to be a valuable tool in visualising the tethering and fusion of vesicles containing glycosylation enzymes to their targeted cisternae. Furthermore, the simplicity of the cell free assay allows for testing of various cellular components on their effect on vesicle tethering without the influence of other cellular factors.

## Aims

This project aims to develop the tools required for the study of targeting, tethering, and fusion of vesicles, using the Golgi as a model system with TIRFM. This will be achieved through developing stable cell lines expressing tagged B4GALT1 and MGAT1 glycosylation enzymes for use in future cell-free experiments to determine the functions, interactions and timings of tethering factors within the Golgi, including the COG. This project also aims to establish a protocol to utilise TIRFM to quantify the intensity of single fluorophores relative to their distance from the slide surface, data which can be extrapolated to future cell-free experiments in order to quantify the movement of vesicles to the Golgi cisternae.

# Materials and Methods

## Plasmid Preparation Through Digestion

This project used the plasmids pDelta UCOE GFP (provided by R.Sizer, University of York), and pHTC HaloTag CMV-neo vector (Promega, 9PIG771). Restriction enzymes utilised are shown on Table 1. Restriction digestion of plasmids were carried out according to recommended incubation temperatures, times and suitable buffers on NEB website (pDelta UCOE GFP: add 0.77µl of DNA to 5µl rCutsmart buffer, 1µl NheI-HF, 42µl H2O, incubate at 37°C for 15 minutes, then add 100mM NaCl and 1µl SalI and incubate at 37°C for 15 minutes. pHTC HaloTag CMV-neo: add 2µl DNA to 5µl 3:1 buffer, 1µl EcoRV, 42µl H2O, incubate at 37°C for 15 minutes, (New England Biolabs, 2023)). Agarose gel electrophoresis to select for the truncated vector backbones was conducted on a 1% agarose gel stained with SYBR Safe DNA Gel Stain (ThermoFisher Scientific, S33102) along with a DNA ladder (Thermo Scientific GeneRuler 1kb Plus DNA Ladder). DNA was extracted following the freeze and squeeze method: band is cut out of gel, placed in a 0.2 micron filter insert column, frozen at -20°C for 5 minutes, centrifuged, frozen again, and repeated until all the DNA is collected at the bottom of the tube.

| Restriction enzyme | Source |
|---|---|
| **NheI-HF** | NEB #R3131 |
| **SalI** | NEB #R0138 |
| **EcoRV** | NEB #R0195 |
| **XhoI** | NEB, #R0146 |
| **BSU36I** | NEB, #R0524 |
| **AfeI** | NEB, #R0652 |
| **AhdI** | NEB #R0584 |
| **FspI** | NEB #R0135 |

***Table 1 – Restriction enzymes used in this study.***

## Primer Design and PCR

PCR was carried out for SNAPTag (pSEMXT-26m plasmid, NEB), B4GALT1 (plasmid provided by D.Ungar, University of York), and MGAT1 (plasmid provided by D.Ungar, University of York) to introduce overlapping edges to coding sequences for Gibson assembly. Primers were designed to introduce overlapping complementary edges to adjascent fragments for Gibson assembly, as well as the Kozak sequence and a Gly/Gly/Ala linker between MGAT1 and SNAPTag (Table 2).

| Primer name | Sequence (5'--->3') | $T_m$ |
|---|---|---|
| **MGAT1 F Primer** | GTTAAGTTAACGGCCGGCCGCTAGCCTCGAG GCCACCATGCTGAAGAAGCAGTCTGCAGG | 59.6°C |
| **MGAT1 R Primer** | AAGCTTTCCGGCGGCTCCGGCGGCTCCGGCA TTCCAGCTAGGATCATAGCCCTCC | 59.7°C |
| **SNAPTag F Primer** | GCCGGAGCCGCCGGAGCCGCCGGAAAGCTTA TGGACAAAGACTGCGAAATGAAGC | 60.9°C |
| **SNAPTag R Primer** | CTTGCATGCCTGCAGGTCGATCTAGATTACTA ACCCAGCCCAGGCTTGCC | 63.2°C |
| **B4GALT1 F Primer** | GATCGCTTCCGAATTCCTACCGCGGATATCG CCACCATGAGGCTTCGGGAGCCGCTC | 64.2°C |
| **B4GALT1 R Primer** | GCAGGAATTGGGCCCAAATCTAGATGTCGAC CTAGCTCGGTGTCCCGATGTC | 59.4°C |
| **Green = Gly/Gly/Ala linker** | Blue = Complementary to original coding sequence | Red = Kozak sequence / Yellow = Complementary overhangs for Gibson assembly |

***Table 2* - Oligonucleotide primers for PCR.** Note there is no HaloTag primer sequence as that is already included in the pHTC HaloTag vector backbone and does not need amplification.

Reaction volumes were 50µl (Table 3) and used Verifi Mix Polymerase (PCRBIO, PB10.43-01), following the PCRBIO protocol, and included a primers only control, template only control, forward primer only control, and reverse primer only control. Samples were run on a PCR Thermocycler following protocol on Table 4.

| | Volume required for a 50µl reaction | Final concentration |
|---|---|---|
| **2X PCRBIO Verifi Mix Polymerase** | 25µl | 1X |
| **F Primer (10µM)** | 2µl | 400nM |
| **R Primer (10µm)** | 2µl | 400nM |
| **Template DNA (1/10 dilution from stock)** | 1µl | Unknown |
| **$H_2O$** | Up to 50µl | |

***Table 3*** **– Reaction volumes and concentrations for PCR.**

| | Temperature | Time | Cycles |
|---|---|---|---|
| **Hot start** | 98°C | 1 min | X1 |
| **Denaturation** | 98°C | 15 secs | X5 |
| **Annealing** | 62°C | 15 secs | |
| **Extension (30secs/kbp)** | 72°C | 2 mins | |
| **Denaturation** | 98°C | 15 secs | X30 |
| **Annealing** | 70°C | 15 secs | |
| **Extension (30secs/kbp)** | 72°C | 2 mins | |
| **Final extension** | 72°C | 5 mins | X1 |
| **Hold** | 4°C | | ∞ |

***Table 4*** **- PCR protocol for thermocycler.**

PCR products were run on a 1% agarose gel and bands containing the products of interest were analysed for concentration and extracted using the freeze and squeeze method. A minimum concentration of 0.02pmol is required for Gibson assembly (Table 5). PCR products with too low of a concentration underwent ethanol precipitation to increase concentration: add one tenth of the volume of DNA of 3M sodium acetate (pH 5.2), add 2.5 times the total volume of ice cold 100% ethanol, freeze at -20°C overnight, centrifuge at full speed for 30 minutes at 4°C, remove supernatant and wash with ice cold 70% ethanol twice, air dry pellet for 15 minutes, add required volume of water.

| Fragment | Size | Minimum/maximum pmol of DNA | Minimum/maximum ng of DNA |
|---|---|---|---|
| **pDelta GFP vector** | 4661bp | 0.02pmols<br>0.5pmols | 62ng<br>1538ng |

| | | | |
|---|---|---|---|
| **pHTC HaloTag vector** | 6185bp | 0.02pmols | 82ng |
| | | 0.5pmols | 2041ng |
| **MGAT1** | 1402bp | 0.02pmols<br>0.5pmols | 19ng<br>463ng |
| **B4GALT** | 1267bp | 0.02pmols<br>0.5pmols | 17ng<br>418ng |
| **SNAPTag** | 608bp | 0.02pmols<br>0.5pmols | 8ng<br>201ng |

***Table 5*** **- Minimum/Maximum picomoles (pmol) and nanograms (ng) of fragments required for Gibson assembly.**

### Gibson Assembly

Fragments were mixed on ice with Gibson assembly mastermix (exonuclease, polymerase, and DNA ligase, add proper names and volumes) at different ratios of insert:vector following the volumes on Table 6, and incubated at 50°C for one hour.

| **B4GALT1-HaloTag** | **2:1 insert:vector** | **3:1 insert:vector** | **No fragment control** | **Vector only control** |
|---|---|---|---|---|
| **HaloTag vector** | 1.64µl | 1.64µl | 0µl | 1.64µl |
| **B4GALT1 insert** | 1.64µl | 2.36µl | 0µl | 0µl |
| **Gibson assembly mastermix** | 10µl | 10µl | 10µl | 10µl |
| **Water** | 6.72µl | 6µl | 10µl | 8.36µl |
| **Total volume** | 20µl | 20µl | 20µl | 20µl |
| | | | | |
| **MGAT1-SNAPTag** | **2:1 insert:vector** | **No fragment control** | **Vector only control** | |
| **pDelta vector** | 1.24µl | 0µl | 1.24µl | |
| **MGAT1 insert** | 1.38µl | 0µl | 0µl | |
| **SNAPTag insert** | 1.38µl | 0µl | 0µl | |
| **Gibson assembly mastermix** | 10µl | 10µl | 10µl | |
| **Water** | 6.72µl | 10µl | 8.76µl | |
| **Total volume** | 20µl | 20µl | 20µl | |

***Table 6*** **- Volumes mixed for Gibson assembly for B4GALT1-HaloTag and MGAT1-SNAPTag.**

## Confirming Gibson Assembly

Gibson assembled plasmids were transfected into competent *E.coli* cells (NEB, NEB5αC2987H) following recommended protocol from NEB (thaw NEB5αC2987H cells on ice for 10 minutes, add 2µl DNA to cell mixture, flick 5 times to mix, put on ice for 30 minutes, heat shock at 42°C for 30 seconds, put on ice for 5 minutes, add 950ml of LB broth, keep at 37°C for 60 minutes, mix by inverting 5 times, dilute 10X in LB broth then add 50µl to an agar plate (New England Biolabs, 2022)) and grown at 37°C overnight on ampicillin agar plates. Colonies were picked, outgrown in 10ml LB broth and miniprepped to isolate DNA following the Promega Wizard Plus SV Miniprep DNA Purification Systems protocol (pellet cells by centrifuging at maximum speed for 5 minutes, discard supernatant and resuspend in 250µl resuspension solution, add 250µl cell lysis solution, invert 4X to mix, add 10µl alkaline protease solution, invert 4X to mix, incubate for 5 minutes at room temperature, add 350µl neutralising solution, invert 4X to mix, centrifuge for 10 minutes at maximum speed, move cell lysate to spin column, centrifuge for 1 minute at maximum speed and remove flow through, add 750µl wash solution, centrifuge for 1 minute at maximum speed, remove flow through and centrifuge for 2 minutes at maximum speed, move column to collection tube, add 100ml H2O and centrifuge for 1 minute at maximum speed (Promega, 2010)).

Correct Gibson assembly was confirmed initially though restriction enzyme digestion (Table 1) to remove the inserts from the vectors to confirm their expression, following recommended incubation temperatures, times and suitable buffers on NEB website (B4GALT1-HaloTag: mix 10µl of midiprepped DNA with 5µl of 3:1 buffer, 1µl XhoI, 1µl EcoRV, 33µl H2O, incubate at 37°C for 30 minutes. MGAT1-SNAPTag: mix 10µl of midiprepped DNA with 5µl rCutsmart buffer, 1µl BSU36I, 1µl AfeI, 33µl H20, incubate at 37°C for 30 minutes, (New England Biolabs, 2023)). These digests were run on an analytical 1% agarose gel to identify colonies with the correct sized fragments.

After identifying the colonies expressing the inserted fragments the plasmids were sequenced to confirm the orientation and correct DNA sequence. Samples were sent for Sanger sequencing to Eurofins Genomics either with primers for MGAT1-SNAPTag (Table 7), or Eurofin's T7 promoter primer for B4GALT1-HaloTag, and plasmids expressing the correct coding sequences in the correct orientation were selected for transfection.

| Primer name | Sequence (5'--->3') | $T_m$ |
|---|---|---|
| **MGAT1 F Primer for sequencing** | CCCTCCCGATACTAGGATCG | 55.9°C |
| **MGAT1 R Primer for sequencing** | CCGACTAATACTAGATCTCAGCG | 54.0°C |
| **SNAPTag F Primer for sequencing** | CCCTCCCGATACTAGGATCG | 55.9°C |
| **SNAPTag R Primer for sequencing** | CCGACTAATACTAGATCTCAGCG | 54.0°C |

***Table 7*** - **Primers used for Sanger sequencing.**

## Cells

HEK293 WT cells (provided by S.Hubbard, University of York) were cultured in an incubator at 37°C 5% $CO_2$ in Dulbecco's Modified Eagle Medium (DMEM)(ThermoFisher Scientific, 11965092) supplemented with 1% Penicillin-Streptomycin (5,000 U/mL, ThermoFisher Scientific, 15070063), 10% FBS (Sigma Aldrich, F7524) and 1% GlutaMAX Supplement (ThermoFisher Scientific, 35050061). Cells were subcultured at a ratio of 1:8 every 3-4 days.

## Transfection and Generation of Stable Cell Lines

Correctly identified recombinant plasmids were re-transfected into C29251 *E. coli* and midiprep isolation was used to collect high quality copies of the plasmid following the PureYield Plasmid Midiprep System protocol (pellet cells by centrifuging at maximum speed for 10 minutes, discard supernatant and resuspend in 3ml cess resuspension solution, add 3ml cell lysis solution, invert 5X to mix, incubate for 3 minutes at room temperature, add 5ml neutralisation solution, invert 10X to mix, centrifuge at 15,000g for 15 minutes, add supernatant to column and allow to flow through with gravity, add 10ml column wash solution to the column and allow to flow through repeat by adding another 10ml column wash solution, move column to collection tube and add 400µl H20 to elute DNA (Promega, 2023)). Plasmids were linearised with restriction enzymes (Table 1). Wild-type

HEK293 cells were grown to 80% confluency in a 6 well plate. HP X-tremeGENE DNA Transfection Reagent (Sigma Aldrich, XTGHP-RO) was mixed with plasmid DNA (Table 6) and incubated for 15 minutes before introducing to HEK293 cells and incubating for 48 hours.

| | HP XtremeGENE DNA Transfection Reagent | 2.4µg DNA | Serum-free medium |
|---|---|---|---|
| **B4GALT1-HaloTag** | 6µl | 32µl (75ng/µl) | Up to 100µl |
| **MGAT1-SNAPTag** | 6µl | 23µl (104ng/µl) | Up to 100µl |
| **Untransfected cells control** | 0µl | 0µg | 100µl |

***Table 8*** **- Volumes used for HEK cell transfection.**

Transfected cells were then split into 10cm plates at dilutions 1:1, 1:10, 1:100, and 1:1000, with 1:1 conditioned media: fresh media along with either G418 (800µg/ml) for B4GALT1-HaloTag transfections, or Puromycin (0.75µg/ml) for MGAT1-SNAPTag transfections. Cells were grown until colonies were visible at 100X magnification, with media changes every 4 days. Colonies were picked using 1000µl pipette tip rings and moved to 24 well plates where after growing to 100% confluency were split for further western blot and confocal microscopy analysis, as well freezing of cell aliquots in freezing media (90% FBS/10% DMSO).

### Preparation of Cell Lysates

100% confluent transfected HEK293 cells in 24 well plates (240,000 cells) were washed three times with 1ml PBS and lysed with 30µl lysis buffer (50mM Na HEPES, 150mM NaCl, 5mM EDTA, 1% (v/v) Triton X-100, 5.15ml H2O, one cOmplete mini EDTA-free Protease Inhibitor Tablet (Sigma Aldrich, 11836170001), pH 7.4), then homogenised by pulling through 25Xg and 26Xg needles 10 times and 2 times respectively. Samples were centrifuged at 13000rpm for 15 minutes at 4C and pellet was discarded, then supernatant was added 1:1 to 2x Laemmli Sample Buffer (Bio-Rad, 1610737) and heated at 65°C for 10 minutes. Samples were stored at -20°C.

## SDS-PAGE Gel Electrophoresis

SDS-PAGE electrophoresis was carried out using a 12% SDS-PAGE gel in a chamber with 1X SDS PAGE running buffer (diluted from 10X SDS PAGE running buffer: 30g TRIS base, 144g glycine, 10g SDS into 1000ml H20) and PageRuler Prestained Protein Ladder (ThermoFisher Scientific, 26616), at 120v for 10 minutes then increased to 150v until the dye front reached the bottom of the gel (around 45-60 minutes).

## Western Blot Analysis

SDS-PAGE gel was transferred to a PVDF membrane via the semi dry transfer method (8ml semi dry transfer buffer (60 mM Tris, 40 mM CAPS buffer, pH 9.6), 20ml methanol, 172ml dH2O, layer with transfer membrane between thick blotting paper onto transfer machine and run at 0.3A for 60 minutes). The membrane was then blocked for one hour in 5% milk powder in 1X PBS-T (100ml 10XPBS, 1ml Tween, into 900ml H20), and probed with antibodies in 2.5% milk powder in 1X PBS-T (Table 9). Each antibody was incubated separately for one hour and washed three times with 1X PBS-T after probing. Membrane was imaged using iBright Imaging System (ThermoFisher Scientific) by adding 2ml SuperSignal West Pico Plus ECL (ThermoFisher Scientific, 34580). Western blots were imaged using the iBright Imaging System with exposure times of 10 seconds (B4GALT1 blot), and 3 minutes (GAPDH blot).

| Antibody | Concentration | Source |
|---|---|---|
| **Mouse anti-B4GALT1** | 1:2000 | ThermoFisher Scientific, MA5-30078 |
| **Mouse anti-GAPDH** | 1:2000 | Sigma Aldrich, G8795 |
| **Goat anti-Mouse IgG HRP** | 1:2000 | ThermoFisher Scientific, 31430 |

***Table 9** - Antibodies used for western blot.*

## Confocal Microscopy of Transfected Cells

The HEK cells successful stably transfected with B4GALT1-HaloTag were selected for confocal microscopy to confirm B4GALT1-HaloTag localisation. The method for confocal microscopy is adapted from Fisher *Et al.,* (2019). Multiple slides were created with varying combinations of antibodies and nocodazole.

60,000 transfected HEK cells were seeded onto poly-lysine treated coverslips in a 24 well dish. After 24 hours cells were treated with 5mM nocodazole for 3 hours, followed by fixation in 4% paraformaldehyde, labelling with 1:1000 HaloTag ligand Oregon Green (Promega, G2802) for 15 minutes, washing with PBS, and blocking with blocking buffer (0.1% saponin (x/v), 2% BSA (w/v), 20mM glycine in 1X PBS). Cells were labelled with trans-Golgi marker mouse antibody TGN38 (100µl 1:500 in 2% milk in 1X PBS) and incubated for 30 minutes at room temperature, then washed four times with 1X PBS. Secondary antibody AF568 goat anti-mouse (100µl 1:500 in 2% milk in 1X PBS) was then added to cells and incubated for 30 minutes at room temperature, then washed four times with 1X PBS. Finally, GM130-AF647 mouse antibody (100µl 1:500 in 2% milk in 1X PBS) was added to cells followed by repeating the incubation and washing steps. Cells were stained with 1:2000 DAPI for 2 minutes at room temperature, washed three times in 1X PBS, and coverslips were transferred to blue roll to air dry. Coverslips were mounted onto 1mm slides by adding one drop of ImmunoFluoroMount (GeneTex, GTX30930-GTX) and transferring onto slides, then cured in the dark overnight before imaging.

Assay images were obtained using either the ZEISS LSM 980 Confocal Microscope or the ZEISS LSM 880 Airyscan Confocal Microscope with a 63x oil immersion objective. During image acquisition power and gains of individual excitation laser lines were adjusted by eye to maximise fluorescence output. For image aquisition a continuous scan speed of 8 was used at a resolution of 512x512 pixels. Once in focus, a single scan was initiated using an image size of 44.9µmX44.9µm, a pixel size of 0.07µm, sampling of 1.0x, a scan speed of 8, and single line averaging of either 8 or 16. Images were analysed using ZEISS ZEN BLUE 3.8.

**TIRFM Slide Preparation**

Varying concentrations of B4GALT1-YFP vesicles (provided by D.Ungar, University of York) were analysed either for their YFP or with a FM1-43 membrane stain. 25X 5µm diameter silica beads were sonicated to mix, then 2µl was diluted to 1X in 48µl of H2O. 2µl of the 1X silica bead solution was mixed with 39.7µl KHM buffer (100mM KCl, 10mM HEPES pH7.2, 2.5mM $Mg(OAc)_2$), and 5µl FM1-43 dye for the slides requiring dye, otherwise this was omitted for the YFP slides. 3.3µl of B4GALT1-YFP vesicles from a frozen stock were added to create a 15X dilution of vesicles. These solutions were added to either uncoated or poly-lysine coated quartz slides (20µg polylysine/1ml in MOPS buffer) and a coverslip was added and secured using clear nail varnish.

Further experiments included a wash step after the addition of the diluted vesicles to the slides, where the coverslip was secured only on two sides with nail varnish and 30µl of KHM buffer was pulled through the open sides by capillary action twice, followed by sealing the other two sides of the coverslip with varnish.

### TIRFM Image Acquisition

B4GALT1-YFP vesicle slides were visualised with an in-house modified inverted Zeiss IM35 chassis fitted with a 100x oil-immersion objective (Zeiss Plan-Apochromat, NA 1.4). TIRFM illumination was provided by a 488nm (30mW) optically pumped solid-state laser (Sapphire LP, Coherent). An image splitter (Optosplit II, Carin Research) split the fluorescent images into two channels with a dichroic beam splitter (FT580, Zeiss) and band pass filters for YFP (ET525/50M, Chroma) and FM1-43 (HQ605/70M, Chroma). 900 frame videos were collected with a 33ms exposure (30 fps) at scale 10.4167 pixels/µm, and 15 videos were collected for each slide for analysis. All video data was collected at room temperature (20-22°C).

### TIRFM Data Processing

All videos were 3-frame median filtered to reduce background noise using an existing program implemented in MATLAB R2021a (written by Rosalyn Leaman, University of York). Following this, ImageJ analysis was used to determine number of vesicles per video, and the intensity and area of each vesicle. For each video, a Z project was created containing frames 1 to 100 of each video. The first 100 frames of the 900 frame video were used to minimise the effects of photobleaching on vesicle detection.

A background threshold was set manually for each set of videos collection from a given sample to capture as many individual vesicles as possible and particles were analysed to determine the number of vesicles in each z-stack as well as their areas and mean intensity (Figure 7). Data was exported to Excel where the data was filtered to remove the higher intensity/area values in order to remove vesicles that were too close together and read as one large vesicle. The threshold for this selection was calculated by plotting the area/intensity of vesicles for each video individually, then adding a line of best fit and calculating the $R^2$ value, followed by removing the highest values until the $R^2$ is 0.65 or higher, indicating the removal of data outliers. Intensity/area was then calculated in Excel and counts

of these values were plotted on a histogram. The optimal histogram bin width and bin number were calculated using the Freedman-Diaconis statistical test (Freedman and Diaconis, 1981).

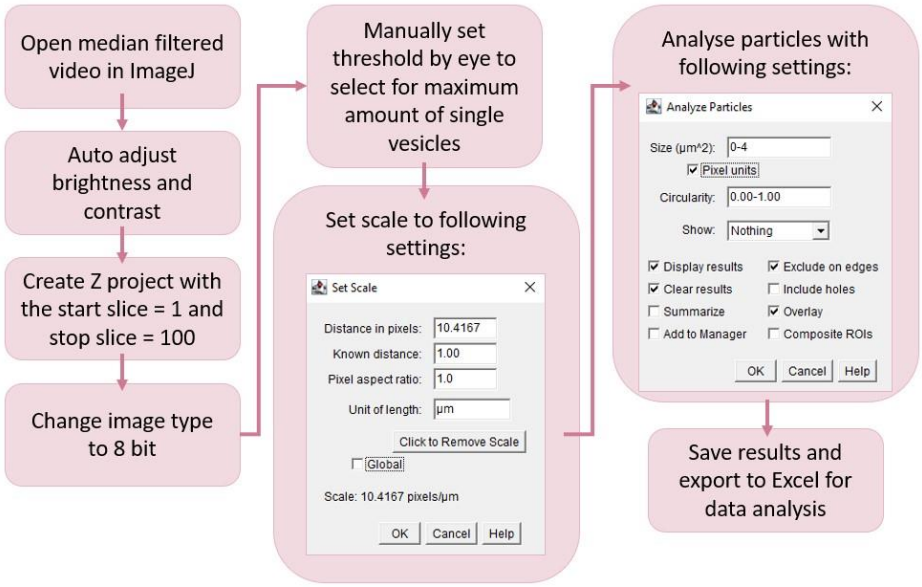


***Figure 7*** **- Protocol and settings followed for ImageJ analysis of area and mean for individual vesicles from TIRF microscopy data.**

Further PaTrack analysis was completed to track individual vesicle intensities over time (Figure 8). Data was exported to Excel, and vesicle intensity versus time plots were created for each individual tracked vesicle.

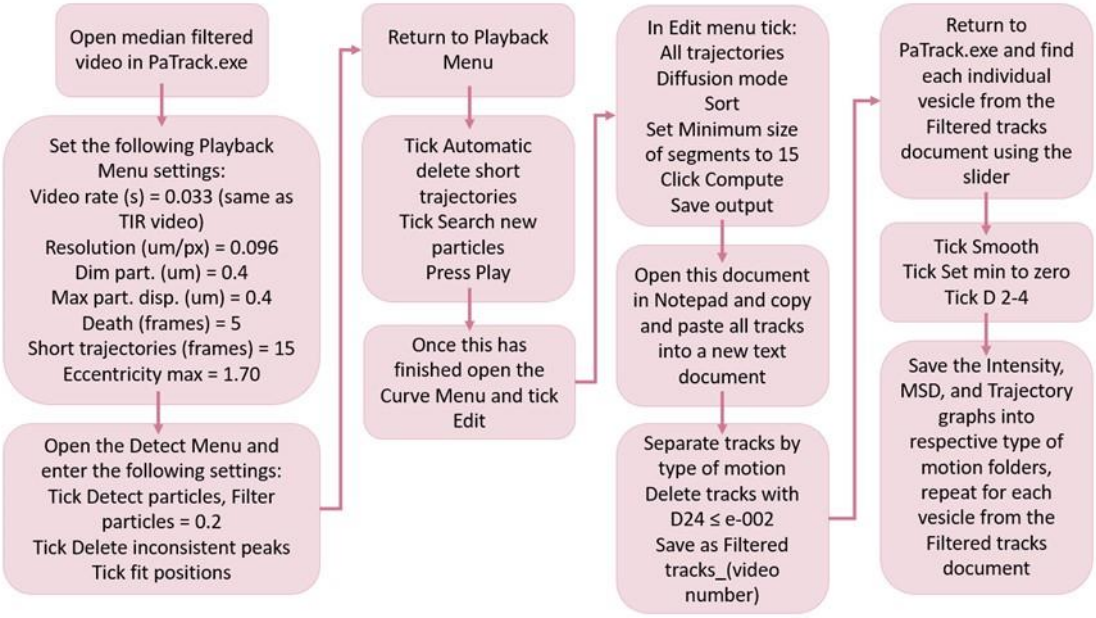


***Figure 8*** **- Protocol and settings followed for PaTrack analysis of vesicle intensity/time.**

# Development and Validation of Stable Cell Lines Expressing Tagged Glycosylation Enzymes

## Introduction

This project aims to develop a method to visualise the movement, tethering and fusion of intra-Golgi vesicles between the cisternae stacks. The development of an assay which allows for this clear visualisation will lay the foundation for future experiments where the specific mechanisms controlling intracellular movement can be analysed. For the development of this assay, two glycosylation enzymes within the Golgi were selected for fluorescent tagging: B4GALT1 and MGAT1. These two enzymes were selected because they are localised to separate cisternae of the Golgi stack, meaning vesicles containing B4GALT1 will tether and fuse to the trans-Golgi cisternae, and MGAT1 vesicles will fuse to medial-Golgi cisternae. This specificity can later be exploited in future experiments, as disruptions to known tethering factors can be introduced and their effects on vesicle specificity can be visualised, furthering our understanding on how they influence intra-golgi vesicle movement. In order to set up this assay, B4GALT1 was tagged with HaloTag, and MGAT1 was tagged with SNAPTag. The development of stable cell lines expressing these tagged glycosylation enzymes will allow for the investigation of medial and trans intra-Golgi vesicle tethering and fusion to the Golgi cisternae, utilising a mixture of vesicles with different fluorescent tags to distinguish their movement during live TIRFM imaging.

The plan for the tagging of these glycosylation enzymes was to generate stable HEK293 cells lines expressing B4GALT1-HaloTag and MGAT1-SNAPTag. This has been achieved through Gibson assembly of the coding sequences for the glycosylation enzymes to the tags, followed by their transfection into HEK293 cells, antibiotic selection, and validation through western blot analysis and confocal microscopy.

### Plan and Vector Backbone Preparation Through Digestion

In order to generate stable cell lines expressing B4GALT1-HaloTag and MGAT1-SNAPTag, plasmids need to be generated expressing these proteins. MGAT1-SNAPTag was assembled from multiple sources: pDelta UCOE GFP as a backbone, MGAT1, and SNAPTag from pSEMXT-26m plasmid. The vector pDelta UCOE GFP was prepared for Gibson assembly with MGAT1 and SNAPTag through the removal of the GFP coding region with restriction enzymes NheI-HF and SalI (Figure 9a). This product was run on an agarose gel to identify the two separate fragments: pDelta UCOE vector (4661bp) and GFP (720bp). This gel was cut to remove the band of interest so an image was not taken of it. Similarly, the vector pHTC HaloTag CMV-neo was linearised with EcoRV before the HCMV promoter for Gibson assembly with B4GALT1 (Figure 9b).

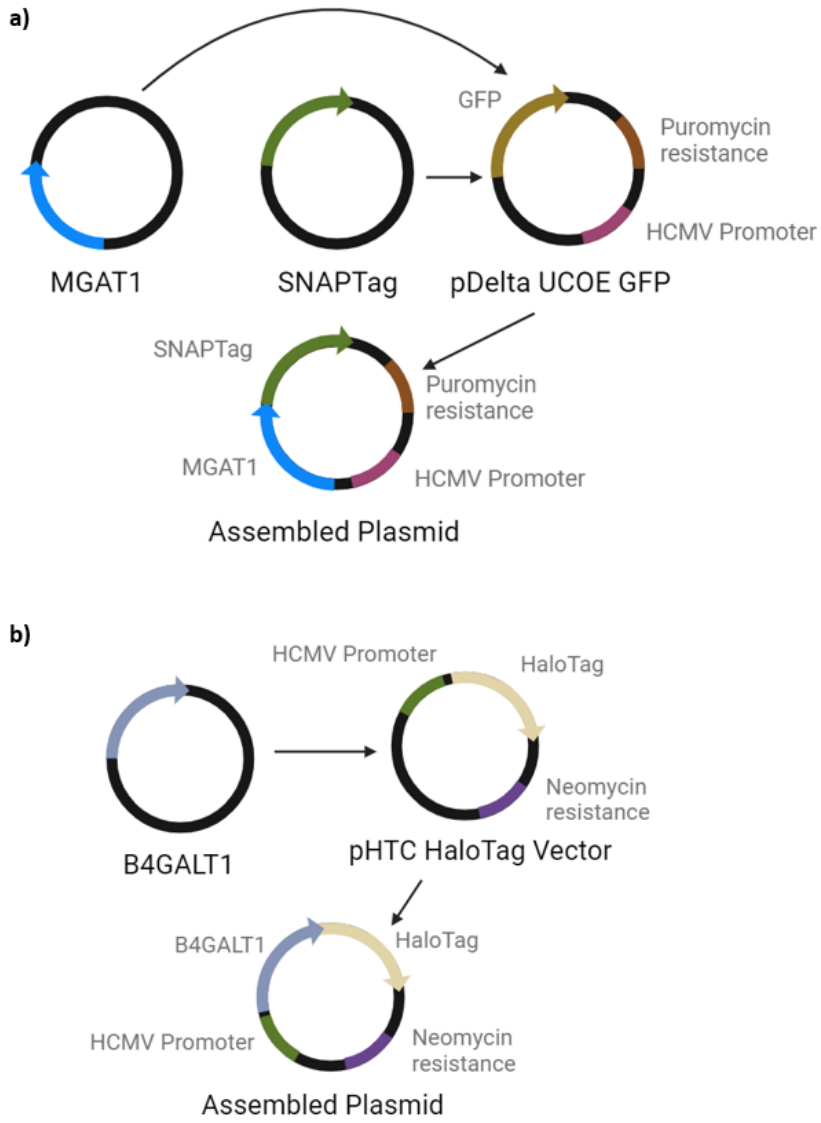


***Figure 9*** **- Plans for plasmids preparation.** a) MGAT1 and SNAPTag to be inserted into pDelta UCOE GFP. b) B4GALT1 to be inserted into pHTC HaloTag Vector.

## PCR Preparation of Insert Fragments

PCR was conducted for MGAT1, SNAPTag, and B4GALT1 with primers containing complementary overhangs for Gibson assembly, as well as the Kozak sequence to enhance translation initiation, and a Gly/Gly/Ala linker between MGAT1 and SNAPTag to provide flexibility. Following PCR, products were run on an agarose gel to determine concentrations. From comparing the band brightness to the known concentration of the ladder bands, MGAT1 is shown to have a concentration of around 40ng/µl, B4GALT1 has a concentration of around 10ng/µl, and SNAPTag has a concentration of around 50ng/µl (Figure 10). For Gibson assembly a higher concentration of MGAT1 and B4GALT1 fragments was required, so ethanol precipitation was conducted to generate final concentrations of 100ng/µl MGAT1 and 100ng/µl B4GALT1.

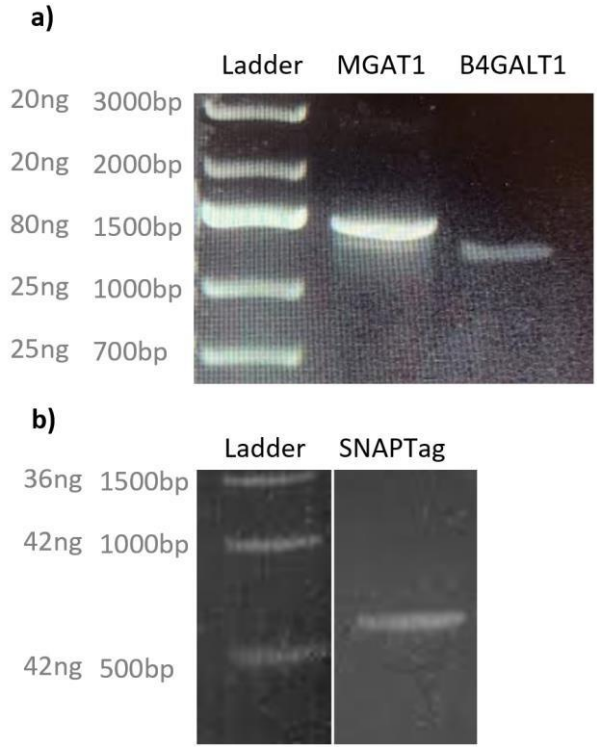


***Figure 10*** - **Agarose gel electrophoresis results for PCR products.** MGAT1 and B4GALT1 (a), and SNAPTag (b). 5µl of ladder was loaded along with 2µl of each PCR product for concentration analysis.

## Confirming Gibson Assembly

Following the assembly of the B4GALT1-HaloTag and MGAT1-SNAPTag plasmids, restriction enzymes were used to separate the plasmids into fragments which were then analysed on agarose gels in order to confirm the successful generation of the plasmids (Figure 11, Figure 12). For the B4GALT1-HaloTag plasmid, the size of the fragments after digestion with XhoI and EcoRV are 6185bp and 1267bp.Minipreps 1-6 are shown to contain the correct fragments from Gibson assembly (Figure 11a, Figure 12a), and further Sanger sequencing of all these clones identified miniprep 2 to contain the full correct coding sequence for B4GALT1-HaloTag (Figure 13a), however only the first 1141 base pairs were successfully sequenced, leaving the last 90bp of B4GALT1 unsequenced.

For the MGAT1-SNAPTag plasmid, the size of the fragments after Bsu36I and AfeI digestion are 1453bp and 5114bp. Agarose gel shows minipreps 2, 3, 8 and 9 contain the correctly assembled plasmids, and the other minipreps most likely contain plasmids either missing fragments or fragments in the incorrect orientation (Figure 11b, Figure 12b). Sanger sequencing confirmed that miniprep 8 expresses the full correct sequence for MGAT1-SNAPTag (Figure 13b).

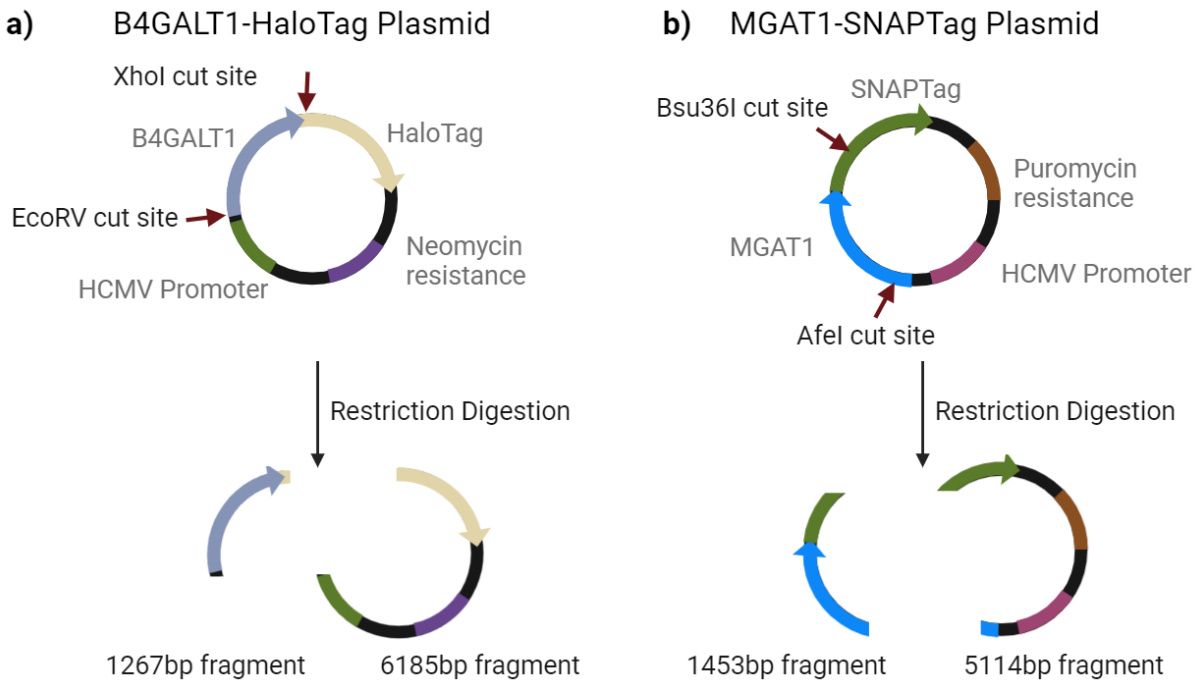


***Figure 11 - Plan of restriction enzyme digestion to confirm insertion of Gibson assembled fragments into vector backbones****. a) Bsu36I and AfeI digested MGAT1-SNAPTag plasmid, and b) XhoI and EcoRV digested B4GALT1-HaloTag plasmid.*

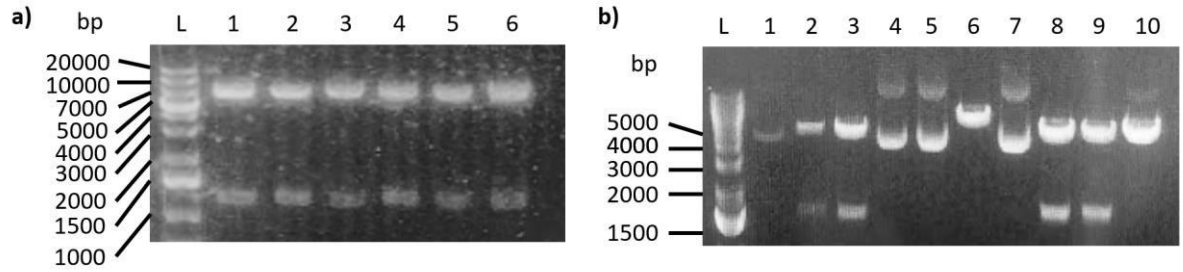


***Figure 12* - Agarose gels of restriction enzyme digested B4GALT1-HaloTag and MGAT1-SNAPTag.** a) Agarose gel of B4GALT1-HaloTag minipreps after XhoI and EcoRV digestion showing two distinct bands for each miniprep at around 6000bp and 1250bp, confirming the presence of B4GALT1 in the HaloTag vector backbone. b) Agarose gel of MGAT1-SNAPTag minipreps after BSU36I and AfeI digestion with lanes 2, 3, 8 and 9 showing bands at around 5000bp and 1500bp, confirming the presence of MGAT1 and SNAPTag in the backbone. Both gels were run at 100V for 45 minutes on a 1% (w/v) agarose gel, alongside the Thermo Scientific™ GeneRuler 1 kb Plus DNA Ladder.

**a) B4GALT1-HaloTag Miniprep2 Sanger Sequencing**

EcoRV Cut Site B4GALT1

```
B4GALT1-HaloTag_Miniprep2_T7_Sequencing     AGTGCTTCGAATTCCTACCGCGGATATCGCCACCATGAGGCTTCGGGAGCCGCTCCTGAG  60
B4GALT1-HaloTag_Theoretical_Sequence        AGTGCTTCGAATTCCTACCGCGGATATCGCCACCATGAGGCTTCGGGAGCCGCTCCTGAG  60
                                            ************************************************************

B4GALT1-HaloTag_Miniprep2_T7_Sequencing     CGGCAGCGCCGCGATGCCAGGCGCGTCCCTACAGCGGGCCTGCCGCCTGCTCGTGGCCGT  120
B4GALT1-HaloTag_Theoretical_Sequence        CGGCAGCGCCGCGATGCCAGGCGCGTCCCTACAGCGGGCCTGCCGCCTGCTCGTGGCCGT  120
                                            ************************************************************

B4GALT1-HaloTag_Miniprep2_T7_Sequencing     CTGCGCTCTGCACCTTGGCGTCACCCTCGTTTACTACCTGGCTGGCCGCGACCTGAGCCG  180
B4GALT1-HaloTag_Theoretical_Sequence        CTGCGCTCTGCACCTTGGCGTCACCCTCGTTTACTACCTGGCTGGCCGCGACCTGAGCCG  180
                                            ************************************************************

B4GALT1-HaloTag_Miniprep2_T7_Sequencing     CCTGCCCCAACTGGTCGGAGTCTCCACACCGCTGCAGGGCGGCTCGAACAGTGCCGCCGC  240
B4GALT1-HaloTag_Theoretical_Sequence        CCTGCCCCAACTGGTCGGAGTCTCCACACCGCTGCAGGGCGGCTCGAACAGTGCCGCCGC  240
                                            ************************************************************

B4GALT1-HaloTag_Miniprep2_T7_Sequencing     CATCGGGCAGTCCTCCGGGGAGCTCCGGACCGGAGGGGCCCGGCCGCCGCCTCCTCTAGG  300
B4GALT1-HaloTag_Theoretical_Sequence        CATCGGGCAGTCCTCCGGGGAGCTCCGGACCGGAGGGGCCCGGCCGCCGCCTCCTCTAGG  300
                                            ************************************************************

B4GALT1-HaloTag_Miniprep2_T7_Sequencing     CGCCTCCTCCCAGCCGCGCCCGGGTGGCGACTCCAGCCCAGTCGTGGATTCTGGCCCTGG  360
B4GALT1-HaloTag_Theoretical_Sequence        CGCCTCCTCCCAGCCGCGCCCGGGTGGCGACTCCAGCCCAGTCGTGGATTCTGGCCCTGG  360
                                            ************************************************************

B4GALT1-HaloTag_Miniprep2_T7_Sequencing     CCCCGCTAGCAACTTGACCTCGGTCCCAGTGCCCCACACCACCGCACTGTCGCTGCCCGC  420
B4GALT1-HaloTag_Theoretical_Sequence        CCCCGCTAGCAACTTGACCTCGGTCCCAGTGCCCCACACCACCGCACTGTCGCTGCCCGC  420
                                            ************************************************************

B4GALT1-HaloTag_Miniprep2_T7_Sequencing     CTGCCCTGAGGAGTCCCCGCTGCTTGTGGGCCCCATGCTGATTGAGTTTAACATGCCTGT  480
B4GALT1-HaloTag_Theoretical_Sequence        CTGCCCTGAGGAGTCCCCGCTGCTTGTGGGCCCCATGCTGATTGAGTTTAACATGCCTGT  480
                                            ************************************************************

B4GALT1-HaloTag_Miniprep2_T7_Sequencing     GGACCTGGAGCTCGTGGCAAAGCAGAACCCAAATGTGAAGATGGGCGGCCGCTATGCCCC  540
B4GALT1-HaloTag_Theoretical_Sequence        GGACCTGGAGCTCGTGGCAAAGCAGAACCCAAATGTGAAGATGGGCGGCCGCTATGCCCC  540
                                            ************************************************************

B4GALT1-HaloTag_Miniprep2_T7_Sequencing     CAGGGACTGCGTCTCTCCTCACAAGGTGGCCATCATCATTCCATTCCGCAACCGGCAGGA  600
B4GALT1-HaloTag_Theoretical_Sequence        CAGGGACTGCGTCTCTCCTCACAAGGTGGCCATCATCATTCCATTCCGCAACCGGCAGGA  600
                                            ************************************************************

B4GALT1-HaloTag_Miniprep2_T7_Sequencing     GCACCTCAAGTACTGGCTATATTATTTGCACCCAGTCCTGCAGCGCCAGCAGCTGGACTA  660
B4GALT1-HaloTag_Theoretical_Sequence        GCACCTCAAGTACTGGCTATATTATTTGCACCCAGTCCTGCAGCGCCAGCAGCTGGACTA  660
                                            ************************************************************

B4GALT1-HaloTag_Miniprep2_T7_Sequencing     TGGCATCTATGTTATCAACCAGGCGGGAGACACTATATTCAATCGTGCTAAGCTCCTCAA  720
B4GALT1-HaloTag_Theoretical_Sequence        TGGCATCTATGTTATCAACCAGGCGGGAGACACTATATTCAATCGTGCTAAGCTCCTCAA  720
                                            ************************************************************

B4GALT1-HaloTag_Miniprep2_T7_Sequencing     TGTTGGCTTTCAAGAAGCCTTGAAGGACTATGACTACACCTGCTTTGTGTTTAGTGACGT  780
B4GALT1-HaloTag_Theoretical_Sequence        TGTTGGCTTTCAAGAAGCCTTGAAGGACTATGACTACACCTGCTTTGTGTTTAGTGACGT  780
                                            ************************************************************

B4GALT1-HaloTag_Miniprep2_T7_Sequencing     GGACCTCATTCCAATGAATGACCATAATGCGTACAGGTGTTTTTCACAGCCACGGCACAT  840
B4GALT1-HaloTag_Theoretical_Sequence        GGACCTCATTCCAATGAATGACCATAATGCGTACAGGTGTTTTTCACAGCCACGGCACAT  840
                                            ************************************************************
```

```
B4GALT1-HaloTag_Miniprep2_T7_Sequencing   TTCCGTTGCAATGGATAAGTTTGGATTCAGCCTACCTTATGTTCAGTATTTTGGAGGTGT   900
B4GALT1-HaloTag_Theoretical_Sequence     TTCCGTTGCAATGGATAAGTTTGGATTCAGCCTACCTTATGTTCAGTATTTTGGAGGTGT   900
                                         ************************************************************

B4GALT1-HaloTag_Miniprep2_T7_Sequencing   CTCTGCTCTAAGTAAACAACAGTTTCTAACCATCAATGGATTTCCTAATAATTATTGGGG   960
B4GALT1-HaloTag_Theoretical_Sequence     CTCTGCTCTAAGTAAACAACAGTTTCTAACCATCAATGGATTTCCTAATAATTATTGGGG   960
                                         ************************************************************

B4GALT1-HaloTag_Miniprep2_T7_Sequencing   CTGGGGAGGAGAAGATGATGACATTTTTAACAGATTAGTCTTTAGAGGCATGTCTATATC   1020
B4GALT1-HaloTag_Theoretical_Sequence     CTGGGGAGGAGAAGATGATGACATTTTTAACAGATTAGTCTTTAGAGGCATGTCTATATC   1020
                                         ************************************************************

B4GALT1-HaloTag_Miniprep2_T7_Sequencing   TCGCCCAAATGCTGTGGTCGGGAGGTGTCGCATGATCCGCCACTCAAGAGACAAGAAAAA   1080
B4GALT1-HaloTag_Theoretical_Sequence     TCGCCCAAATGCTGTGGTCGGGAGGTGTCGCATGATCCGCCACTCAAGAGACAAGAAAAA   1080
                                         ************************************************************

B4GALT1-HaloTag_Miniprep2_T7_Sequencing   TGAACCCCATCCTCAGAGGTTTGACCGAATTGCACACACAAAGGAAACAATGCTCTCTGA   1140
B4GALT1-HaloTag_Theoretical_Sequence     TGAACCCCATCCTCAGAGGTTTGACCGAATTGCACACACAAAGGAAACAATGCTCTCTGA   1140
                                         ************************************************************

B4GALT1-HaloTag_Miniprep2_T7_Sequencing   T  1141
B4GALT1-HaloTag_Theoretical_Sequence     T  1141
                                         *
```

**b) MGAT1-SNAPTag Miniprep 8 Sanger Sequencing**

```
MGAT1-SNAPTag_Miniprep8      TTAGTGAACCGTCAGATCCGCTAGAATTCGAGCTCCCTGCAGGTTAGTTAAGTTAACGGC   60
MGAT1-SNAPTag_Theoretical    TTAGTGAACCGTCAGATCCGCTAGAATTCGAGCTCCCTGCAGGTTAGTTAAGTTAACGGC   60
                             ************************************************************
                                                                                  MGAT1
MGAT1-SNAPTag_Miniprep8      CGGCCGCTAGCCTCGAGGCCACCATGCTGAAGAAGCAGTCTGCAGGGCTTGTGCTGTGGG   120
MGAT1-SNAPTag_Theoretical    CGGCCGCTAGCCTCGAGGCCACCATGCTGAAGAAGCAGTCTGCAGGGCTTGTGCTGTGGG   120
                             ************************************************************

MGAT1-SNAPTag_Miniprep8      GCGCTATCCTCTTTGTGGCCTGGAATGCCCTGCTGCTCCTCTTCTTCTGGACGCGCCCAG   180
MGAT1-SNAPTag_Theoretical    GCGCTATCCTCTTTGTGGCCTGGAATGCCCTGCTGCTCCTCTTCTTCTGGACGCGCCCAG   180
                             ************************************************************
                                                                                  AfeI cut site
MGAT1-SNAPTag_Miniprep8      CACCTGGCAGGCCACCCTCAGTCAGCGCTCTCGATGGCGACCCCGCCAGCCTCACCCGGG   240
MGAT1-SNAPTag_Theoretical    CACCTGGCAGGCCACCCTCAGTCAGCGCTCTCGATGGCGACCCCGCCAGCCTCACCCGGG   240
                             ************************************************************

MGAT1-SNAPTag_Miniprep8      AAGTGACTCGCCTGGCCCAAGACGCCGAGGTGGAGCTGGAGCGGCAGCGTGGGCTGCTGC   300
MGAT1-SNAPTag_Theoretical    AAGTGACTCGCCTGGCCCAAGACGCCGAGGTGGAGCTGGAGCGGCAGCGTGGGCTGCTGC   300
                             ************************************************************

MGAT1-SNAPTag_Miniprep8      AGCAGATCGGGGATGCCCTGTCGAGCCAGCGGGGGAGGGTGCCCACCGCGGCCCCTCCCG   360
MGAT1-SNAPTag_Theoretical    AGCAGATCGGGGATGCCCTGTCGAGCCAGCGGGGGAGGGTGCCCACCGCGGCCCCTCCCG   360
                             ************************************************************

MGAT1-SNAPTag_Miniprep8      CCCAGCCGCGTGTGCCTGTGACCCCCGCGCCGGCGGTGATTCCCATCCTGGTCATCGCCT   420
MGAT1-SNAPTag_Theoretical    CCCAGCCGCGTGTGCCTGTGACCCCCGCGCCGGCGGTGATTCCCATCCTGGTCATCGCCT   420
                             ************************************************************

MGAT1-SNAPTag_Miniprep8      GTGACCGCAGCACTGTTCGGCGCTGCCTGGACAAGCTGCTGCATTATCGGCCCTCGGCTG   480
MGAT1-SNAPTag_Theoretical    GTGACCGCAGCACTGTTCGGCGCTGCCTGGACAAGCTGCTGCATTATCGGCCCTCGGCTG   480
                             ************************************************************

MGAT1-SNAPTag_Miniprep8      AGCTCTTCCCCATCATCGTTAGCCAGGACTGCGGGCACGAGGAGACGGCCCAGGCCATCG   540
MGAT1-SNAPTag_Theoretical    AGCTCTTCCCCATCATCGTTAGCCAGGACTGCGGGCACGAGGAGACGGCCCAGGCCATCG   540
                             ************************************************************

MGAT1-SNAPTag_Miniprep8      CCTCCTACGGCAGCGCGGTCACGCACATCCGGCAGCCCGACCTGAGCAGCATTGCGGTGC   600
MGAT1-SNAPTag_Theoretical    CCTCCTACGGCAGCGCGGTCACGCACATCCGGCAGCCCGACCTGAGCAGCATTGCGGTGC   600
                             ************************************************************

MGAT1-SNAPTag_Miniprep8      CGCCGGACCACCGCAAGTTCCAGGGCTACTACAAGATCGCGCGCCACTACCGCTGGGCGC   660
MGAT1-SNAPTag_Theoretical    CGCCGGACCACCGCAAGTTCCAGGGCTACTACAAGATCGCGCGCCACTACCGCTGGGCGC   660
                             ************************************************************
```

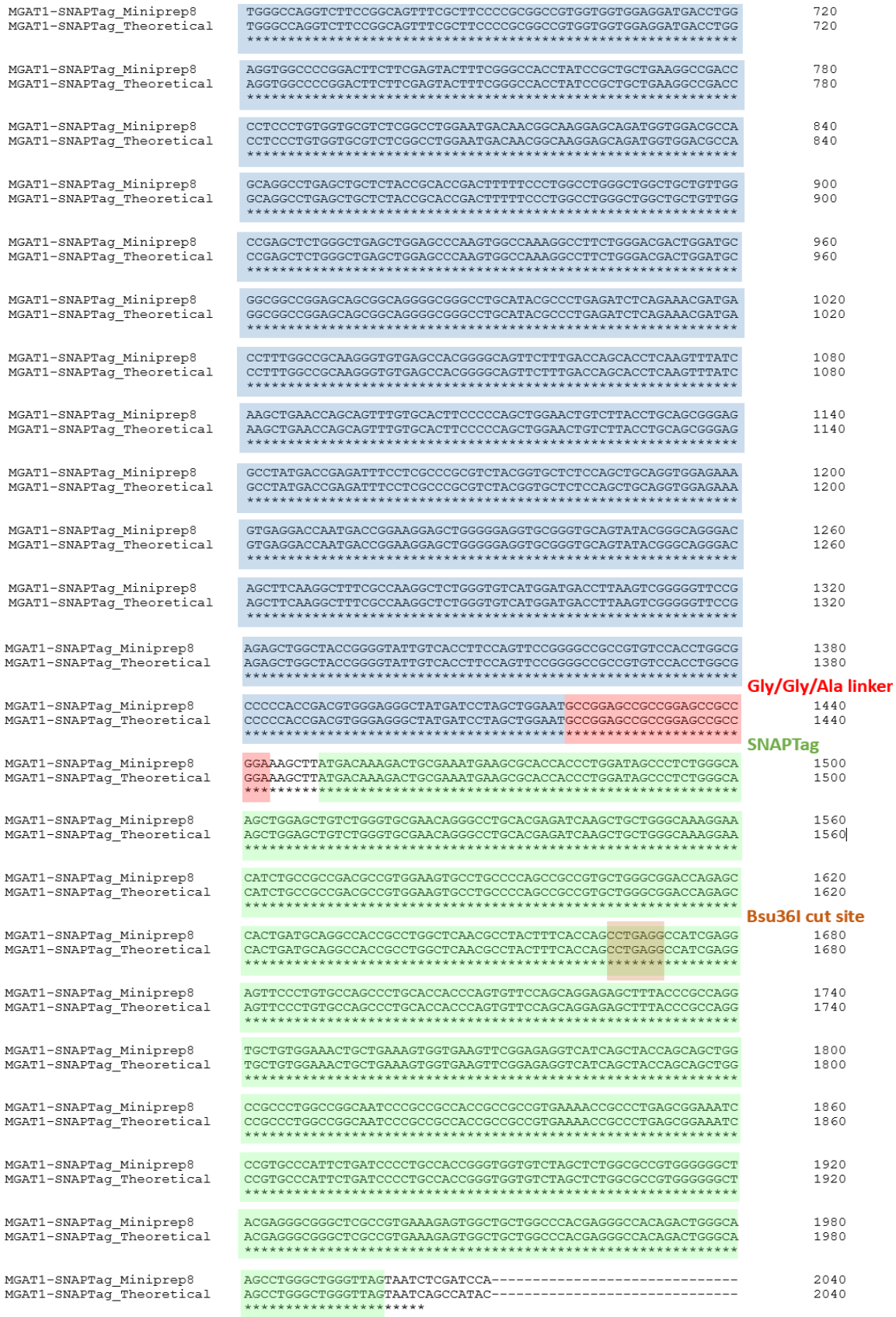


***Figure 13 - Sanger sequencing results***. *(a) B4GALT1-HaloTag showing the B4GALT1 coding region (purple) and EcoRV cut site (yellow), and (b) MGAT1-SNAPTag showing the MGAT1 coding region (blue), SNAPTag coding region (green), AfeI cut site (pink), Bsu36I cut site (orange), and the Gly/Gly/Ala linker (red). A longer sequence read for MGAT1-SNAPTag was achieved through the combination of two separate sequencing runs.*

## Western Blot Analysis of Stable Cell Lines

After the transfection of HEK293 cells with the confirmed B4GALT1-HaloTag plasmid, the cells were outgrown in media containing G418 and 24 total colonies grown were picked for western blot analysis to confirm the expression of the tagged B4GALT1 enzyme (Table 11). Of these picked colonies, 14 grew successfully to confluency in the 24 well plates and were selected for western blot analysis.

| Plate dilution | Number of colonies grown | Number of colonies picked |
|---|---|---|
| **1:1** | >20 | 5 |
| **1:1** | >20 | 5 |
| **1:10** | 9 | 5 |
| **1:10** | 7 | 5 |
| **1:100** | 2 | 2 |
| **1:100** | 3 | 2 |
| **1:1000** | 1 | 0 |
| **1:1000** | 0 | 0 |

***Table 10** - Number of colonies grown and picked from each transfection dilution plate.*

Western blot analysis of HEK293 cell lysate after B4GALT1-HaloTag plasmid transfection (Figure 14a) shows that all cell lines show expression of endogenous B4GALT1 (44kDa) and GAPDH (36kDa), however these are at varying amounts which is reflected in the intensity of the B4GALT1 bands. This may be due to differing volumes of protein expression from the cells, however the presence of GAPDH in each cell line confirms the successful generation of cell lysates. Cell line 3 (B4GALT1-HaloTag_3) is the only cell line to show expression of B4GALT1-HaloTag (77kDa). ImageJ analysis to generate line charts quantifying the intensity of the bands (Figure 14b) shows the area of the line graphs representing the band intensities (highlighted in green) is calculated to be 5471 for B4GALT1-HaloTag, and 27837 for endogenous B4GALT1. This data shows that the B4GALT1-HaloTag band is five times weaker than the intensity of the endogenous B4GALT1 band, Implying that one in six B4GALT1 molecules expressed will be tagged with HaloTag. Additionally, cell lines 4 and 5 show the presence of a protein smaller than B4GALT1 which is most likely non-specific degradation. B4GALT-HaloTag_3 was selected for further confocal microscopy analysis to confirm the localisation of the protein in the Golgi apparatus.

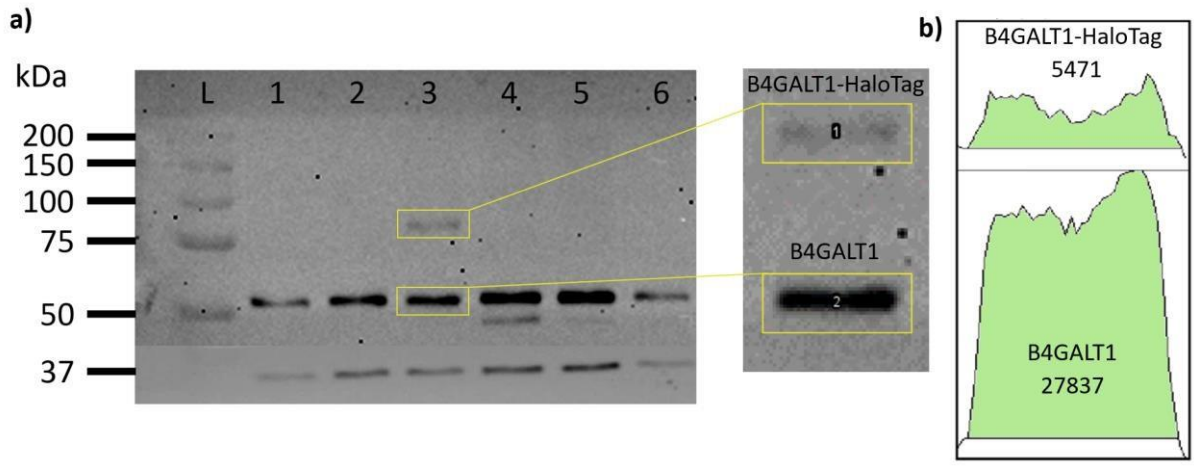


***Figure 14* - Western blot analysis of B4GALT1-HaloTag transfected HEK cells**. a) Western blot of cell lysate for B4GALT1-HaloTag transfected HEK cell lines 1-6 (image cropped to show significant results) and ladder (L) after probing for B4GALT1 and GAPDH with mouse anti-B4GALT1, mouse anti-GAPDH, and goat anti-mouse HRP. b) Image J analysis was used to quantify the intensity of the bands in lane 3.

Following the confirmation of a cell line expressing B4GALT1-HaloTag, these cells then underwent the same method for transfection of MGAT1-SNAPTag so a stable cell line expressing both B4GALT1HaloTag and MGAT1-SNAPTag could be obtained. Unfortunately, during the transfection process, the cells encountered multiple contaminations and died, resulting in an unsuccessful completion of transfection and selection. There was not enough time within this project to repeat the necessary steps to transfect the B4GALT1-HaloTag_3 cells, however all the necessary plasmids and methods are readily available for future work to complete the generation of these stable cell lines.

## Confocal Microscopy of WT HEK and B4GALT1-HaloTag Transfected Cells

Initially, wild type (WT) HEK cells were visualised with confocal microscopy following GM130 and TGN46 antibody staining to refine the process of preparing the slides and confirm the concentrations of antibodies required to visualise the Golgi (Figure 15). These micrographs show the Golgi apparatus localised next to the nucleus of the cells, with a clear distinction between the cisternae of the Golgi containing TGN46 and GM130.

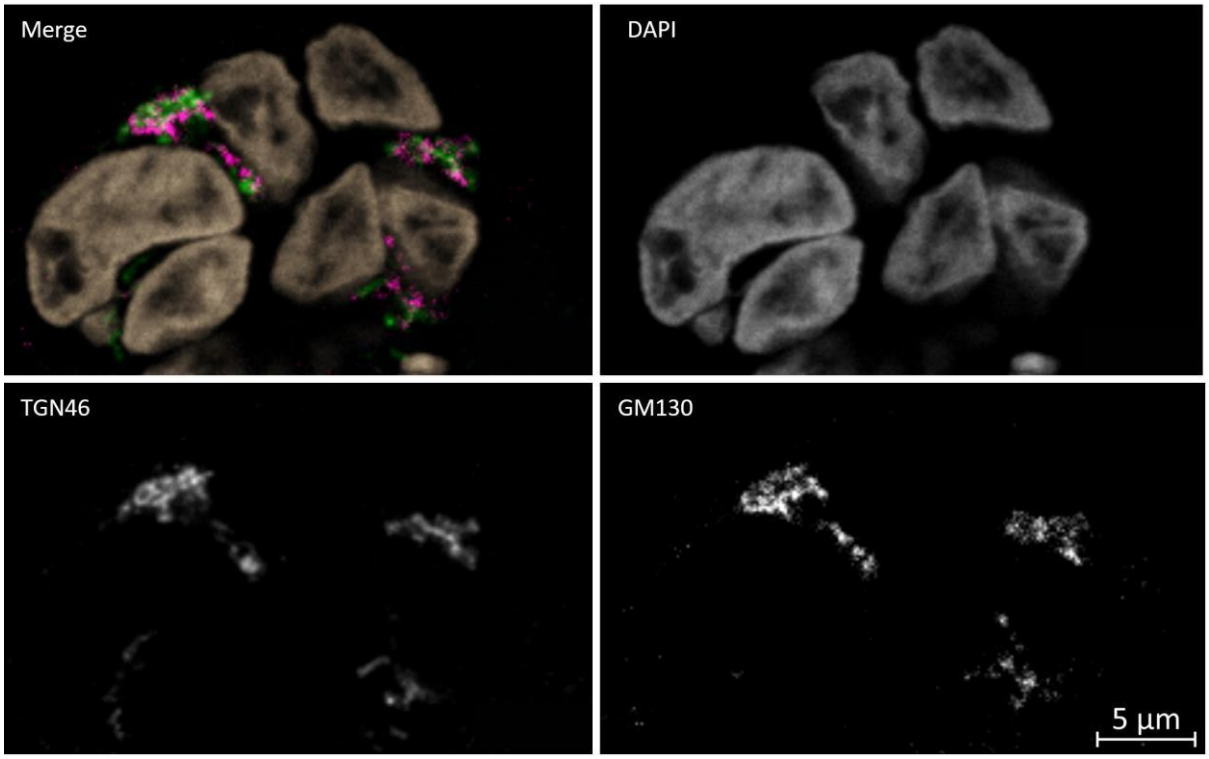


***Figure 15*** *- **Confocal micrograph of wild type HEK cells**. Stained for DAPI (orange), TGN46 (green), and GM130 (magenta) showing the Golgi apparatus located next to the nucleus.*

Following on from WT HEK confocal microscopy, the successfully transfected cells B4GALT1HaloTag_3 were visualised with DAPI, TGN46, GM130, and HaloTag ligand Oregon Green staining to confirm the localisation of the tagged B4GALT1 within the Golgi (Figure 16), as well as a DAPI, TGN46 and GM130 only control (Figure 17). These micrographs also show the distinct TGN46/GM130 containing cisternae with a width between 1µm and 2µm located next to the nucleus as expected, as well as the individual B4GALT1-HaloTag proteins. However, the localisation of B4GALT1-HaloTag is not consistently between TGN46 and GM130 in the Golgi apparatus and is seemingly randomly located within the cell.

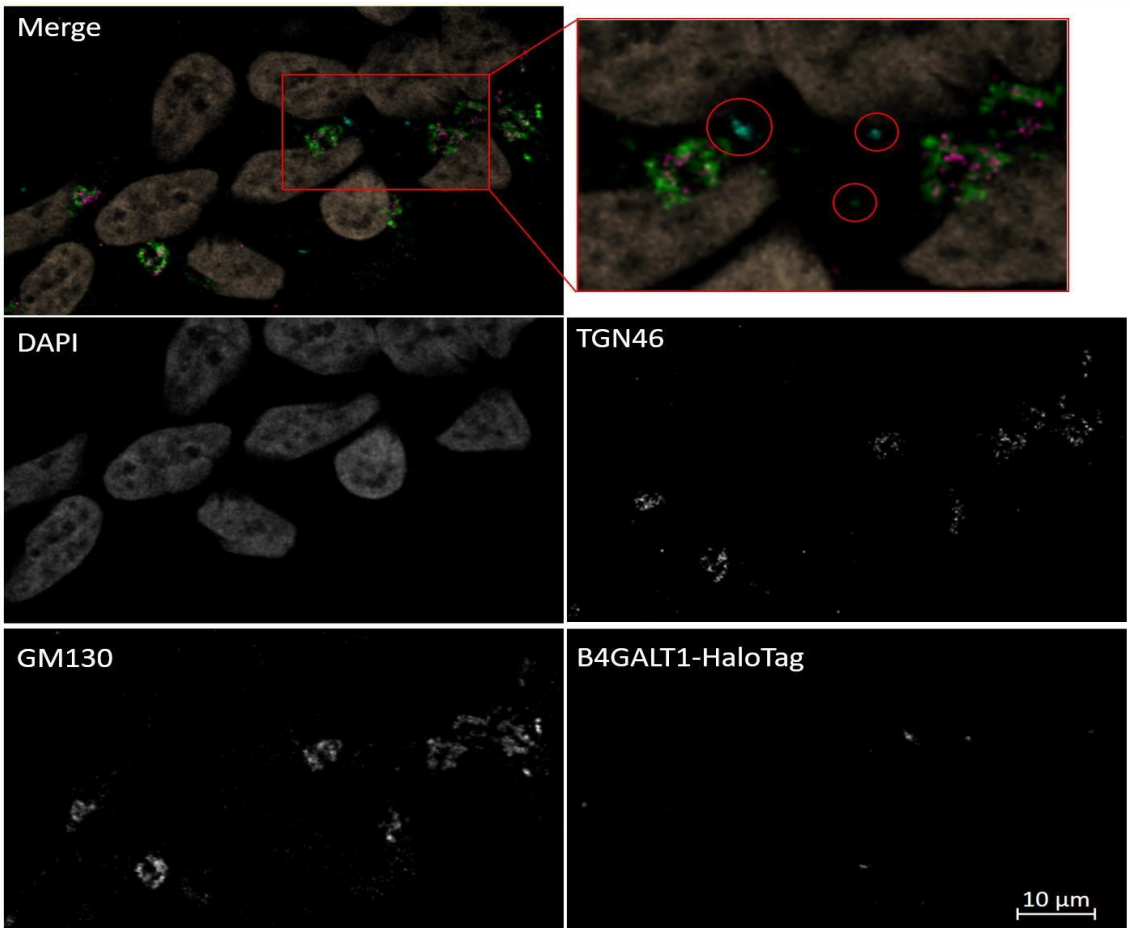


***Figure 16* - Confocal micrograph of B4GALT1-HaloTag_3 cells.** *Stained for DAPI (white), TGN46 (green), GM130 (magenta), and B4GALT1-HaloTag (turquoise) showing the Golgi apparatus localised next to the nucleus with B4GALT1-HaloTag localised elsewhere in the cell.*

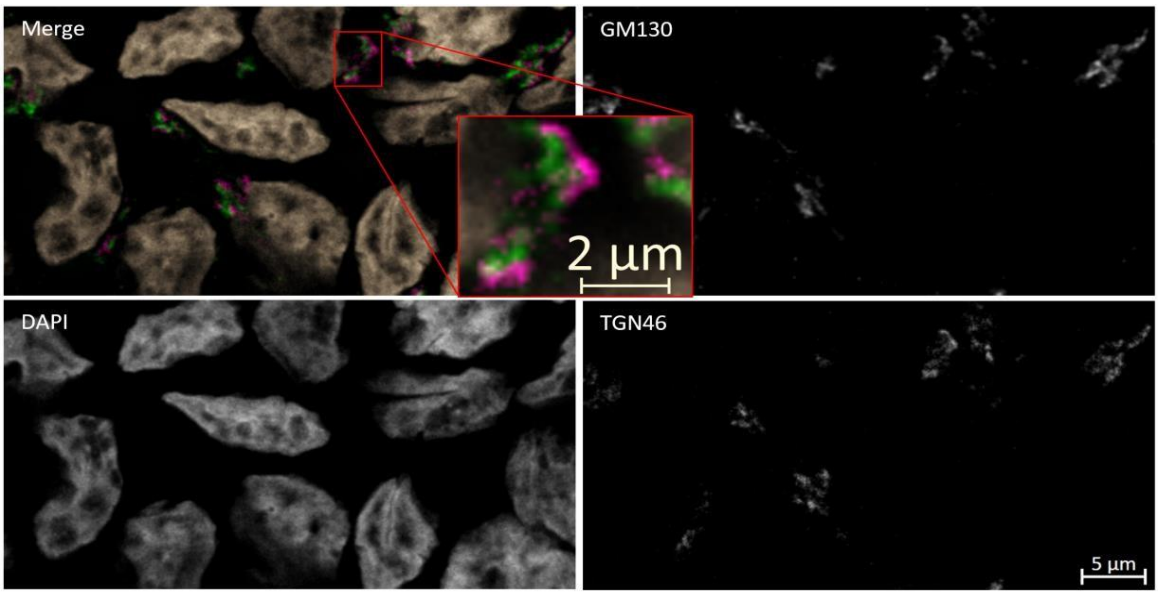


***Figure 17* - Confocal micrograph of B4GALT1-HaloTag_3 cells.** *Stained for DAPI (white), TGN46 (green), and GM130 (magenta) showing the Golgi apparatus is still localised next to the nucleus with distinct cisternae layers.*

In order to confirm if the instances where B4GALT1-HaloTag overlaps with the Golgi apparatus is true localisation or just random, nocodazole treatment was used to induce the formation of ministacks within the Golgi. Ministacks are microtubule independent and are shown to be valid representations of the native Golgi stack. Nocodazole treatment was initially performed on WT HEK cells to confirm the formation of ministacks (Figure 18). These micrographs confirm the formation of nocodazole induced ministacks as highlighted by the red square, showing a ministack of around 1µm in width with cis-Golgi marker GM130 separated from trans-Golgi marker TGN46, highlighting the separation of the Golgi cisternae within the ministack.

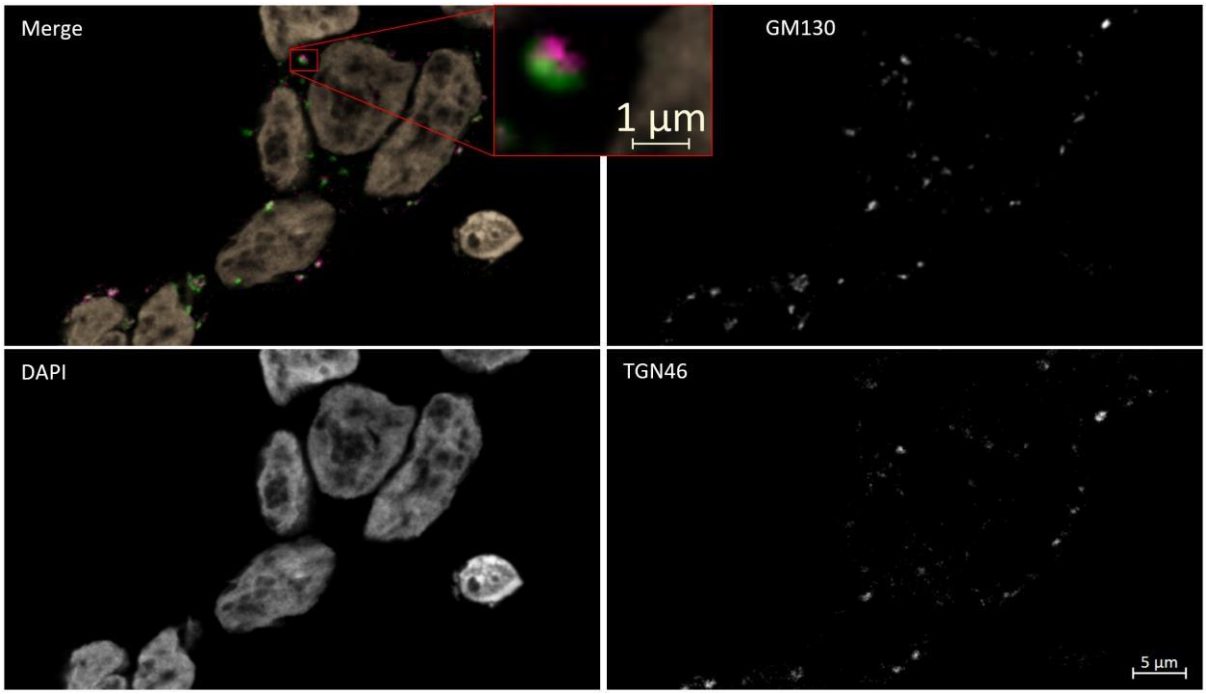


***Figure 18 - Confocal micrograph of ministacks from nocodazole treated WT HEK cells.*** *Stained for DAPI (white), TGN46 (green), and GM130 (magenta) showing multiple distinct Golgi ministacks surrounding the nucleus which retain the separation of glycosylation enzymes between the cisternae.*

Following this confirmation, nocodazole treatment was used on the B4GALT1-HaloTag_3 cells (Figure 19), along with an Oregon free control to confirm the formation of the Golgi ministacks (Figure 20). From this data the Golgi ministacks containing TGN46 and GM130 were visible in the cells in a similar manner to the WT HEK cells. However, the localisation of the B4GALT1-HaloTag is not in the same location as the Golgi ministacks. This confirms that B4GALT1-HaloTag in the B4GALT1-HaloTag_3 cell line is defective and not localising to the Golgi apparatus, as highlighted by the red arrows. The fact that these proteins are visible means that the HaloTag coding region of the proteins are functional and covalently binding to the HaloTag ligand Oregon green, meaning that most likely an error

occurred in the B4GALT1 coding region to impair Golgi retention. From these results these cells are not suitable for the visualisation of intra-Golgi vesicles, and more cells would need to be generated in the future through repeating the transfection steps and selecting for cells where B4GALT1HaloTag is located within the Golgi ministacks between GM130 and TNG46.

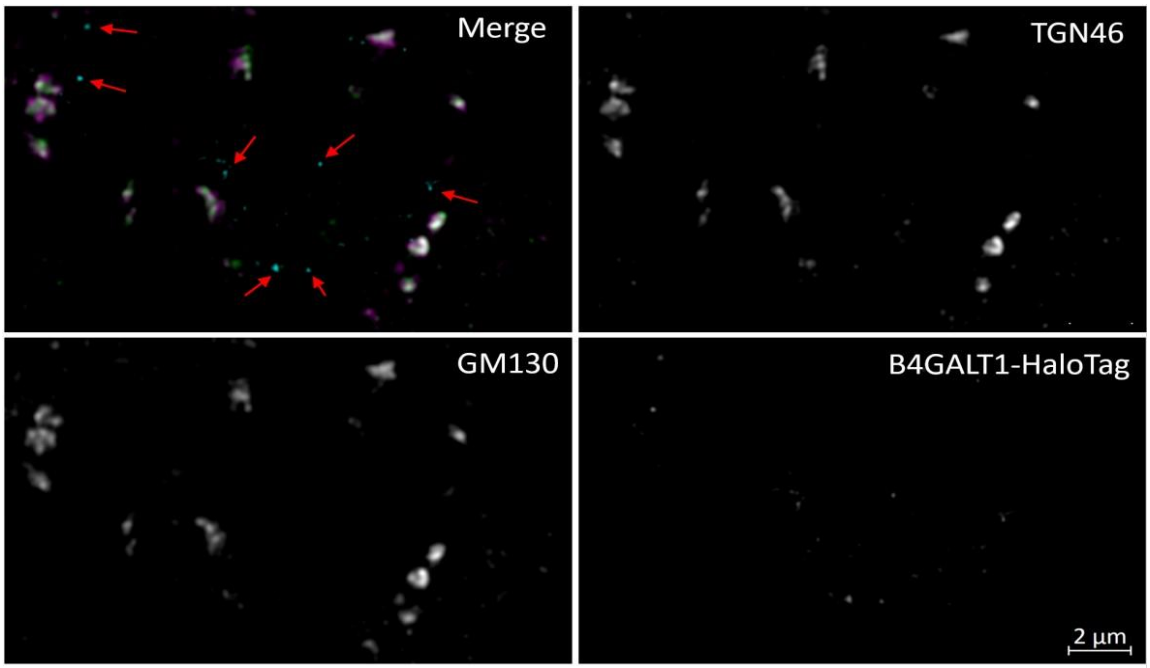


***Figure 19** - Airyscan confocal micrograph of ministacks from nocodazole treated B4GALT1-HaloTag_3 cells. Stained for TGN46 (green), GM130 (magenta), and B4GALT1-HaloTag (Turquoise) showing the localisation of B4GALT1-HaloTag is not in the same location within the cell as the Golgi ministacks.*

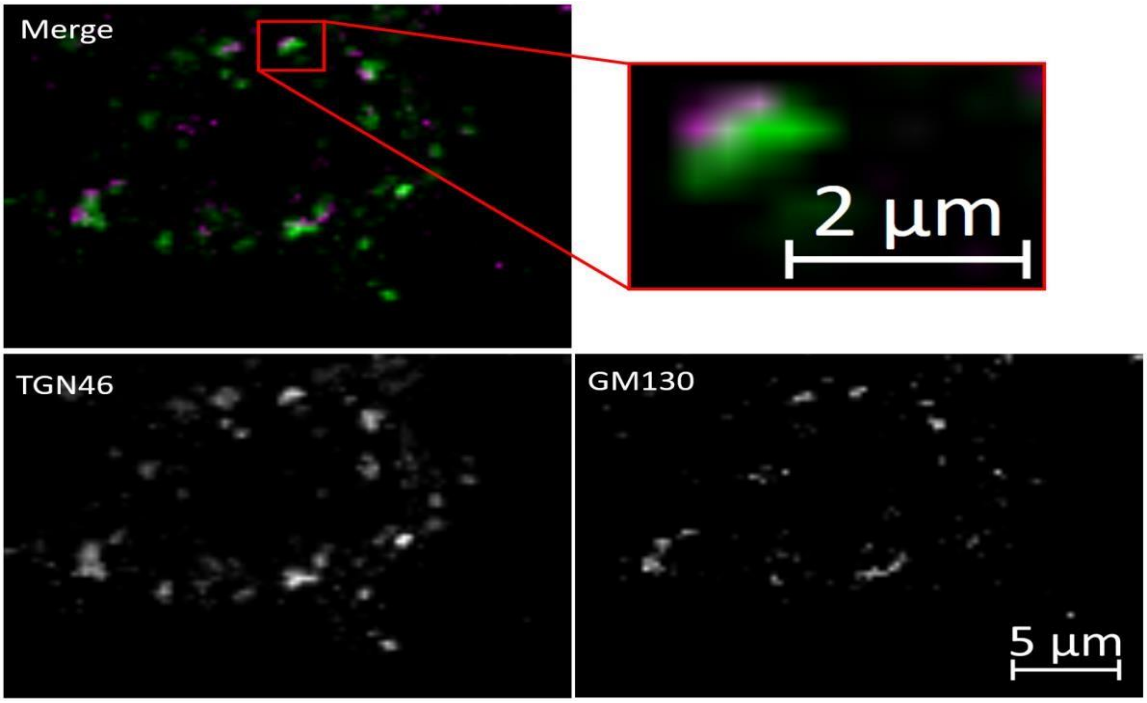


***Figure 20** - Confocal micrograph of ministacks from nocodazole treated B4GALT1-HaloTag_3 cells. Stained for DAPI (white), TGN46 (green), and GM130 (magenta).*

## Conclusion

In order to generate stable cell lines expressing B4GALT1-HaloTag and MGAT1-SNAPTag, plasmids needed to be generated containing the coding sequences for the tagged enzymes. The generation of these plasmids was completed with Gibson assembly, and their contents were confirmed initially though restriction enzyme digestion to analyse the size of the assembled fragments, followed by

Sanger sequencing to verify the plasmids. Following this, B4GALT1-HaloTag was transfected into WT HEK cells, however despite western blot analysis showing the expression of a protein the same molecular weight as B4GALT1-HaloTag, confocal microscopy analysis revealed that B4GALT1-HaloTag did not localise in the Golgi apparatus and therefore was defective.

HaloTag was added to the C terminus of B4GALT1, so the signal peptides on the N terminus which determine protein localisation were not affected. However, it is possible that the addition of the HaloTag could have resulted in a conformational change in the protein structure, leading to the signal peptide no longer being functional and the protein localising to the incorrect sub-cellular location. Furthermore, the Sanger sequencing of B4GALT1-HaloTag did not include the last 90bp of the sequence, so it is possible that a mistake could have been incorporated into the end of the coding region which led to mis-folding of the protein and therefore a loss of function and localisation.

Despite the unsuccessful generation of a stable cell line expressing a functional copy of B4GALT1-HaloTag, this project successfully developed a method for the transfection and confocal microscopy of HEK cells. The identification of the optimal antibiotic concentrations for transfected cell selection, as well as a protocol for the fixing and antibody/Oregon green staining of slides for confocal microscopy was developed during this project, and the methods described can be easily replicated for the future generation of a B4GALT1-HaloTag + MGAT1-SNAPTag cell line.

# TIRFM Imaging of B4GALT1-YFP Vesicles

## Introduction

The calibration and development of a TIRFM imaging method has been completed alongside the generation of tagged glycosylation enzyme expressing cell lines. For these experiments, previously isolated vesicles expressing B4GALT1-YFP were visualised with TIRFM and a method was developed to determine the number of B4GALT1-YFP molecules expressed in each vesicle, as well as the development of a fluorescence intensity versus distance from slide surface calibration curve. This data can then be extrapolated onto the cell free assay of the isolated Golgi cisternae and vesicles from the B4GALT1-HaloTag and MGAT1-SNAPTag transfected HEK cells in order to quantify the approach, tethering and fusion of vesicles to the Golgi cisternae.

## Determining Number of B4GALT1-YFP Molecules in Each Vesicle

In order to confidently develop a fluorescence intensity versus distance from slide surface calibration curve, a method for identifying vesicles containing only one B4GALT1-YFP molecule needed to be developed in order to remove any increased fluorescence intensity detected from vesicles containing more than one B4GALT1-YFP molecule.

Initially, PaTrack analysis was used to generate graphs of intensity over time for individual vesicles on poly-lysine coated slides. This data shows the photobleaching of individual YFP proteins, allowing for the identification of vesicles containing one or two B4GALT1-YFP vesicles, as a reduction in intensity indicates the photobleaching of one YFP as highlighted by the red arrows around every 3 seconds (Figure 21a, 21b). Further analysis on uncoated slides showed vesicles moving freely in solution and measured a higher intensity than the vesicle adsorbed on a poly-lysine coated slide, indicating a higher number of B4GALT1-YFP in some vesicles (Figure 21c). However, the low photostability of YFP led to rapid photobleaching, meaning vesicles containing more than two B4GALT1-YFP were difficult to distinguish.

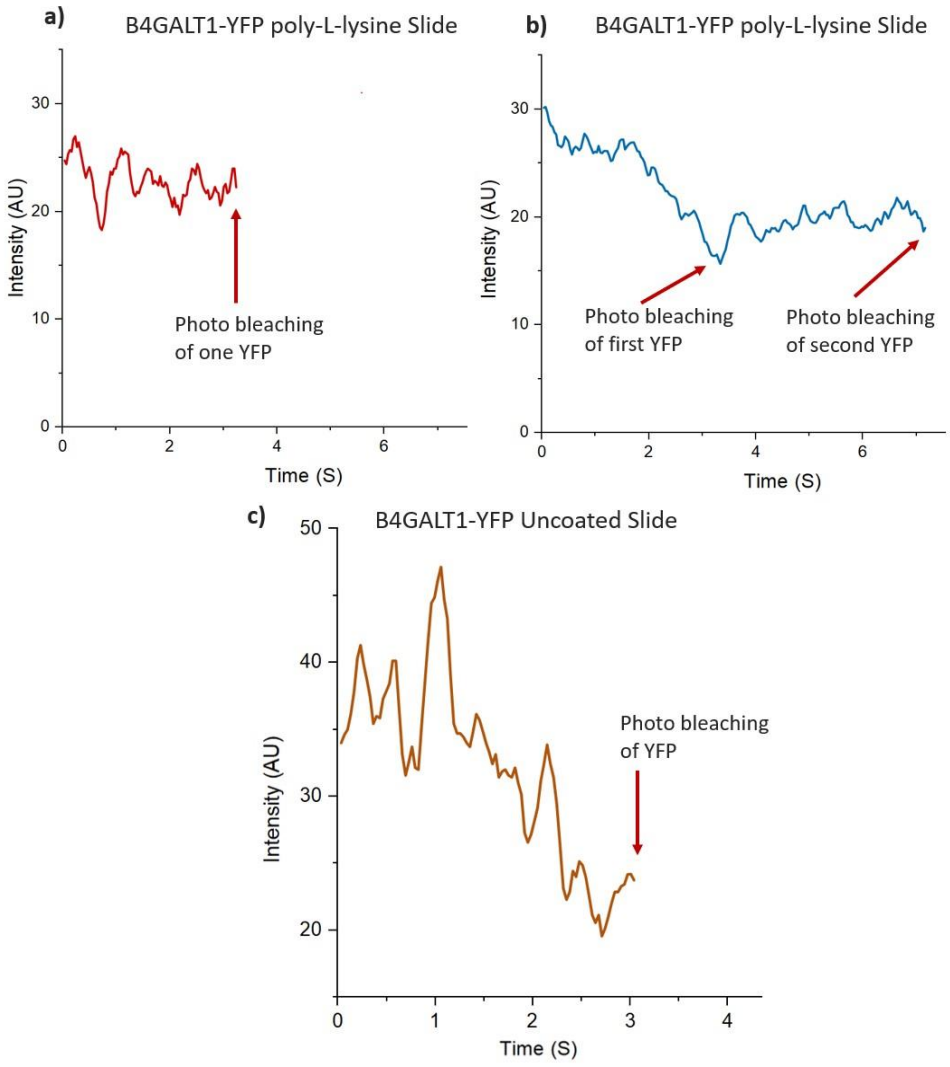


***Figure 21* - *Intensity (AU) over time (S) graphs***. *A single vesicle adsorbed to a poly-lysine coated slide showing the photobleaching of one (a) or two (b) YFP proteins. c) A single vesicle diffusing freely in solution showing a wide range of fluorescence as the vesicle moves through the evanescent field.*

Following this, ImageJ analysis of the sum of the first 100 images from each TIRFM video (Figure 22a) was completed in order to counteract YFP photobleaching, followed by calculating the intensity/area for each vesicle and plotting that data as a histogram (Figure 22b, Supplementary Table 1, Supplementary Table 2). The peaks of the histogram were converted into a line graph based on the count numbers for each bin, and the peaks were deconvoluted using Origin 2023b into separate Gaussian peaks. Each peak represents differing numbers of B4GALT1-YFP in the vesicles, and the average area/intensity of one YFP was set at 300AU (Figure 22c). The area under each curve was calculated and from this data the percentage of vesicles containing differing numbers of YFP molecules was calculated (Figure 22d). From this data it was calculated that 62.61% of the vesicles contained one YFP, 26.37% contained two, 7.60% contained three, and 3.52% contained 4 or more YFP molecules.

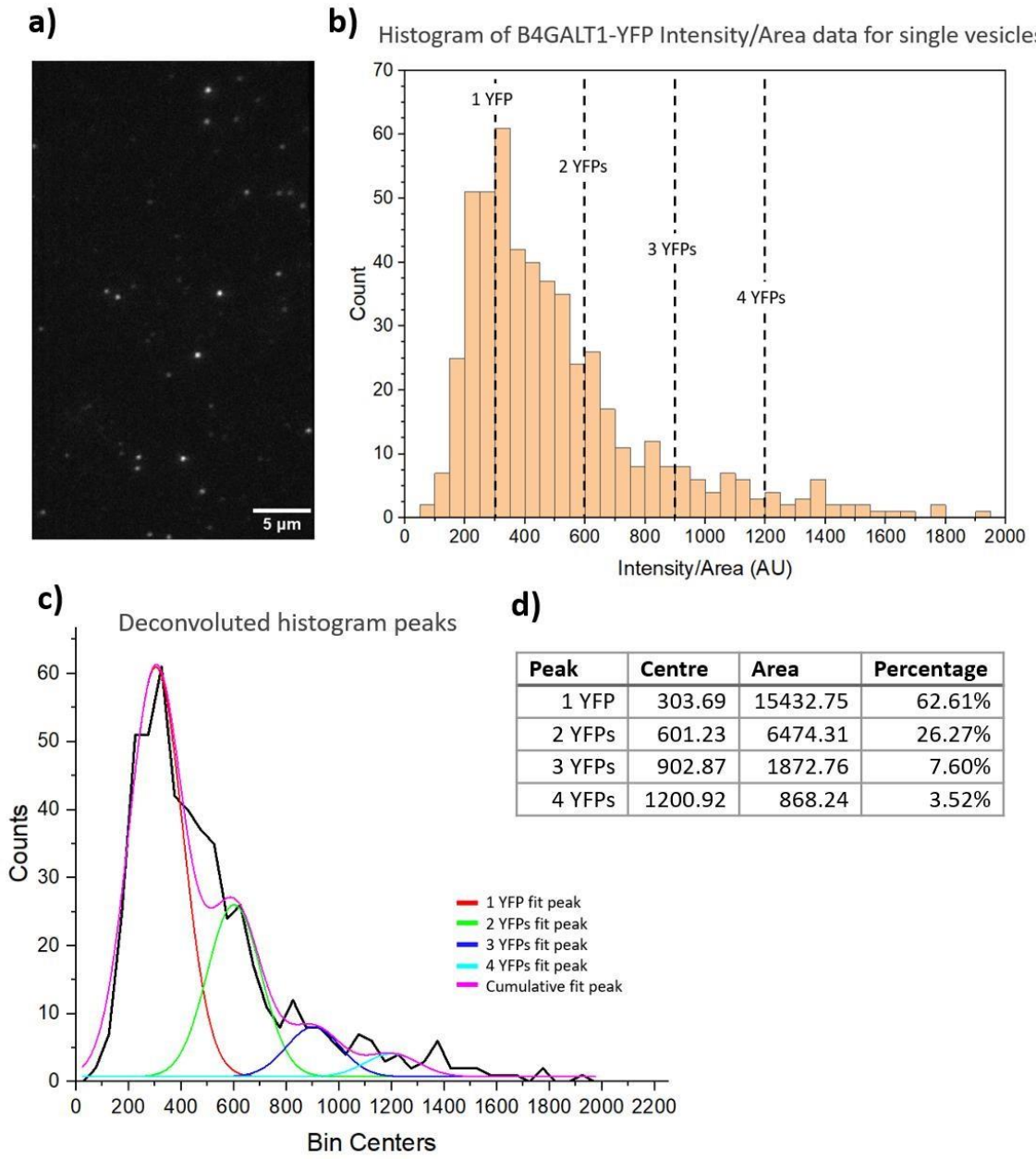


| Peak | Centre | Area | Percentage |
|---|---|---|---|
| 1 YFP | 303.69 | 15432.75 | 62.61% |
| 2 YFPs | 601.23 | 6474.31 | 26.27% |
| 3 YFPs | 902.87 | 1872.76 | 7.60% |
| 4 YFPs | 1200.92 | 868.24 | 3.52% |

***Figure 22 - Analysis of the average number of YFP molecules expressed in B4GALT1-YFP vesicles.*** *a) Example of the sum of the first 100 images from a poly-lysine slide, 100X vesicle dilution, scale bar 5µm. b) Histogram of intensity/area for all single vesicles from 15x sum 100 images. Dotted lines highlight groups of vesicles with differing YFP numbers. c) Histogram converted into line graphs and peaks deconvoluted highlighting differing numbers of B4GALT1-YFPs in individual vesicles. d) Table showing the centre and area of each deconvoluted peak, along with percentages of vesicles with each YFP.*

**Generating Fluorescence Intensity versus Distance from Slide Surface Calibration Curve**

In order to generate a fluorescence intensity versus distance from slide surface calibration curve and therefore accurately measure the distances vesicles move during docking and fusion in 3D, the following assumptions were made: the size of each vesicle was presumed to be 50nm in diameter; when sorting the highest recorded confined intensities from lowest to highest, the lowest 62.61% of these values will be vesicles containing one YFP molecule (as any higher intensities are presumed to be due to multiple YFP molecules); and finally of these vesicles calculated to contain one YFP molecule, the largest of these values will be where the B4GALT1-YFP transmembrane protein is localised closest to the slide surface in the vesicular membrane.

The intensity of one YFP at distance 0nm from the surface of the slide needed to be quantified, as well as the intensity of one B4GALT1-YFP at a known distance from the slide. The intensity at distance 0nm was determined from collating the maximum PaTrack recorded fluorescence intensities for surface immobilised vesicles (on poly-lysine coated slide) and sorting them from lowest to highest values. The lowest 62.61% of these values are presumed to be the fluorescence intensity of one YFP-B4GALT1 at the closest point to the slide surface during random 2D diffusion throughout the vesicular membrane. Of these values, the highest intensity recorded is 48.86 AU, meaning the intensity of one YFP-B4GALT1 molecule at distance = 0nm from the surface of the slide is presumed to be 48.86 AU.

Following this, the lowest intensities from all surface-immobilised vesicles (on poly-lysine coated slide) were collated and sorted from lowest to highest. From these values, the overall lowest intensity was presumed to be the intensity of one YFP-B4GALT1 at the furthest point away from the slide surface, which is 21.12 AU. The size of the vesicles is presumed to be 50nm, so the intensity at distance = 50nm is 21.12 AU. These values were plotted on a graph and an extended exponential line of best fit was added (Figure 23).

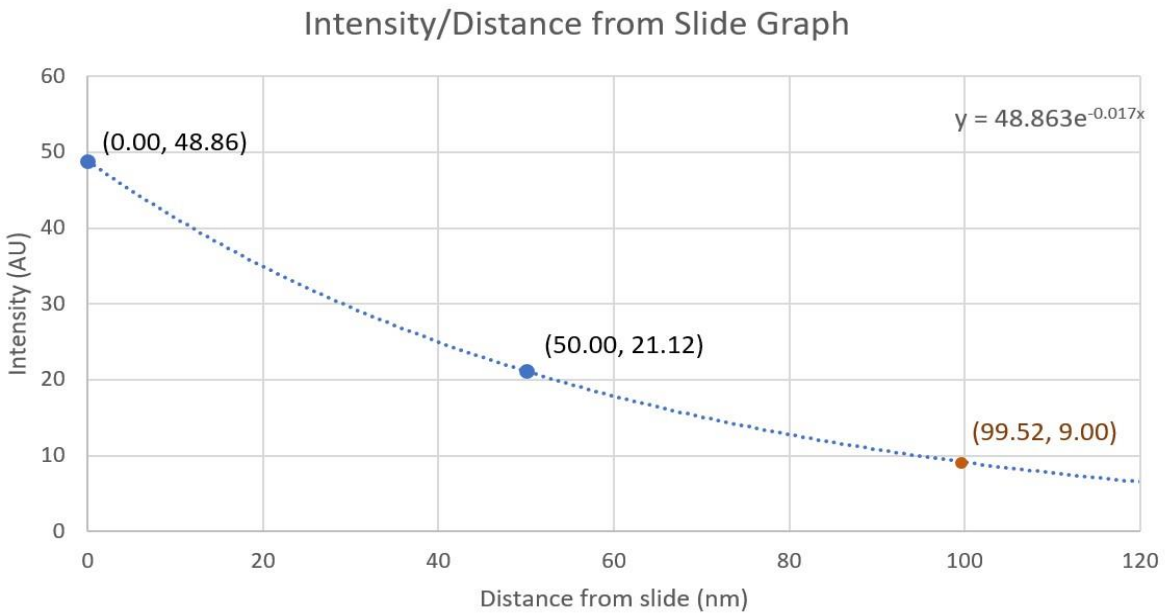


***Figure 23 - Fluorescence intensity versus distance from slide surface calibration curve**. Showing known intensities at distances of 0nm and 50nm, equation of exponential line, and predicted limit of vesicle detection at evanescent field depth of 99.52nm (orange).*

From this data, the maximum distance from the slide surface at which a fluorescently labelled vesicles can be detected was estimated. The lowest recorded intensities from PaTrack data for vesicles on uncoated slides were collated and the lowest of these values was identified to be 9.00 AU. This intensity value is assumed to be the intensity of one YFP-B4GALT1 at the maximum distance from the slide where it can still be sufficiently excited by the evanescent field. Inserting this value into the equation of the exponential line of best fit gives a distance of 99.52nm, as shown in orange (Figure D).

However, inserting the known intensities at distances 0nm and 50nm into an equation to calculate evanescent field depth (Equation 2) shows the depth of the evanescent field to be 68.17nm. This shows a discrepancy as the lowest recorded intensity from the freely diffusing vesicles indicated a distance of 99.52nm from the slide surface, meaning the depth of the evanescent field needs to be at least that distance.

$$I_z = I_0 e^{z/d}$$

***Equation 2 - Equation to determine depth of evanescent field**. $I_Z$ = Intensity at depth z, $I_0$ = Intensity at depth 0, z = distance from slide in nm, d = depth of evanescent field. Inserting known values $I_Z$ = 21.02, $I_0$ = 43.78, z = 50 and rearranging gives d = 68.17. Equation from Fish 2015.*

## Confirming Adhesion of Vesicles on Poly-Lysine Slides

In order to confirm the adhesion of vesicles on the poly-lysine coated slides, the minimum and maximum PaTrack intensity values for each of these surface-immobilised vesicles (labelled as 'confined' particles in Patrack) was collated and plotted as a scatter graph (Figure 24a, 24c). This graph was then compared to the minimum and maximum intensity values for freely diffusing vesicles (labelled as 'Brownian' particles in PaTrack) on the uncoated slides (Figure 24b, 24d). The surface-immobilised vesicles show an overall higher average minimum intensity than the freely diffusing vesicles, which is expected as the uncoated slides will not bind the vesicles as well. The freely diffusing vesicles in these samples will move further away from the surface and out of the most intense region of the evanescent field. Similarly, the maximum intensities are overall higher for the surface-immobilised vesicles which is expected as they are closer to the slide surface and located in the most intense part of the evanescent field.

The purpose of this comparison was to confirm the adsorption of the vesicles to the poly-lysine slide, the expected results would show a wider range of minimum intensities for the uncoated slides compared to the poly-lysine coated slides which suggests less diffusion in the z-direction and therefore the adsorption of the vesicles to the poly-lysine coated slide. However, the poly-lysine coated slides have a higher range between the lowest and highest minimum intensities of 27.42, compared to the uncoated slides which have a range of 23.00.

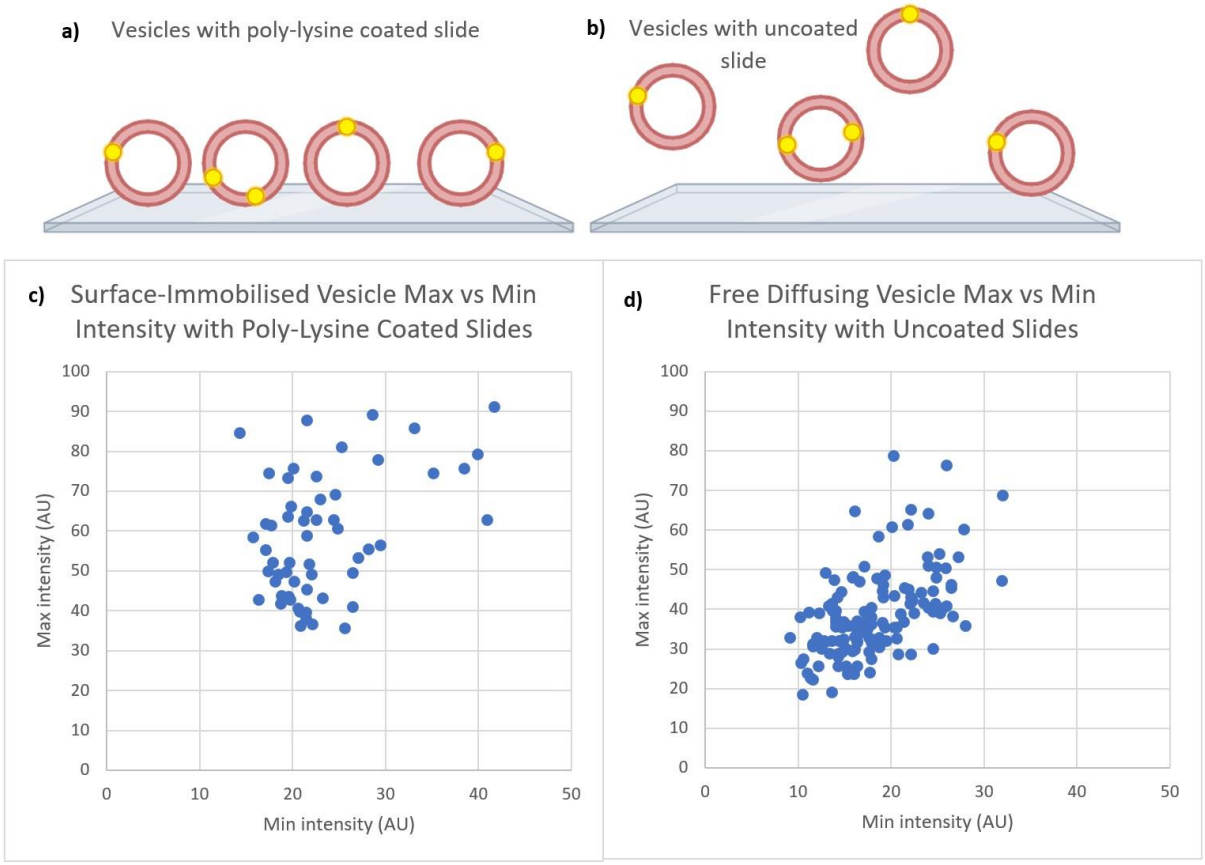


***Figure 24 - Analysis of the adsorption of vesicles to the poly-lysine coated slide****. Schematic of the surface-immobilised vesicles with a poly-lysine coated slide (a), schematic of the freely diffusing vesicles observed with an uncoated slide (b), Scatter graphs showing the minimum against the maximum recorded intensity for each surface-immobilised vesicle with poly-lysine coated slides (c) or a freely diffusing vesicle with uncoated slides (d).*

## Conclusion

The generation of an intensity versus distance from slide graph for TIRFM is a valuable tool in the future analysis of intra-Golgi vesicle tethering and targeting, as the movement of vesicles in the zdirection can now be quantified through their changes in intensity over time. In order to collect this information, a method was developed to identify the number of fluorescent molecules present in each vesicle through analysis of their intensities versus areas. This method can be utilised in future experiments to determine the number of tagged B4GALT1 and MGAT1 enzymes present in isolated vesicles.

# Discussion

## The generation of B4GALT1-HaloTag Expressing Cells

Many proteins have been identified that coordinate intra-Golgi vesicle transport between the cisternae of the Golgi. However, the specific timings of these interactions, and the order in which they interact, are currently unknown. This project aimed to develop the tools required for the visualisation of intra-Golgi vesicle transport with TIRFM, the first step of which is to develop a stable cell line expressing tagged glycosylation enzymes. Previous assays have successfully utilised confocal microscopy to visualise GalT tagged with the fluorescent protein YFP (Fisher *et al.,* 2019), however limitations on the half life of the fluorescent signal reduced the accuracy of their assays. Furthermore, any future assays requiring different or multiple coloured fluorescent tags would require the generation of whole new cell lines, a timely and sometimes unpredictable process. This project proposed the use of HaloTag and SNAPTag to tag glycosylation enzymes B4GALT1 and MGAT1, generating a line of cells which can be readily labelled with a wide array of different coloured fluorophores.

This project successfully generated plasmids expressing B4GALT1-HaloTag and MGAT1-SNAPTag as confirmed by Sanger sequencing, followed by the generation of a stable cell line B4GALT1-HaloTag_3 expressing the B4GALT1-HaloTag plasmid. Confocal analysis revealed that the Golgi apparatus was clearly visible after GM130 and TGN46 staining and visually looked the same as Golgi in the literature (van Bommel *et al.,* 2023). However, after the introduction of HaloTag ligand Oregon green, confocal microscopy showed that the B4GALT1-HaloTag was not localised to the Golgi apparatus, meaning it was not operating how endogenous B4GALT1 would. This was revealed through nocodazole treatment to induce the formation of ministacks in order to confirm if the B4GALT1-HaloTag was part of the Golgi apparatus or randomly located within the cell. This method has previously been used to confirm the order of glycosylation enzymes in the Golgi (Tie *et al.,* 2022).

The lack of localisation of B4GALT1-HaloTag to the ministacks was unexpected as successful transfection of tagged glycosylation enzymes have been previously reported in multiple assays. However, these assays used fluorophores such as YFP (Fisher *et al.,* 2019, Cottam *et al.,* 2014), mCherry (Sørensen *et al*., 2023) or RFP (Schoberer *et al.,* 2013), all of which photo bleach very quickly meaning they were difficult to use in single molecule in vitro assays, highlighting the need for the generation of a new cell line that can be tagged with a more photostable fluorophore. There are multiple reasons the B4GALT1-HaloTag could have not localised to the Golgi, including the

introduction of mutations to the B4GALT1 coding region (Schaub *et al*., Weber *et al.*, 2015) which would affect the localisation of the protein or result in the formation of aggregates. This can be remedied by checking the sequence of the transfected cells in order to confirm if it was the sorting signal that was mutated and following this repeating the experiment to select for more cell lines expressing B4GALT1-HaloTag and checking them with confocal microscopy to confirm their localisation, or potentially a different method for transfection such as mechanical or viral. The addition of the HaloTag to B4GALT1 could also have induced mis-folding of the final protein in a way that disrupts or inactivates the signal peptide, leading to mis-localisation. It has previously been reported that the addition of HaloTag to a protein of interest lead to a loss of function in the protein (Locatelli-Hoops *et al.,* 2013) so it is possible that HaloTag interfered with the function of the recombinant B4GALT1. Alternative tagging methods could be explored in the future, including CLIPTag which is another modified enzyme with multiple fluorescent ligands available. Finally, Sanger sequencing would need to be repeating with a reverse primer in order to sequence the last 90bp of the B4GALT1 coding region which was missed from the original Sanger sequencing. This would rule out the incorporation of incorrect bases into the DNA which would lead to potential mis-folding of the proteins.

While this work did not lead to the discovery of a successful stable cell line, the plasmids and methods for the generation of a B4GALT1-HaloTag + MGAT1-SNAPTag cell lines are readily available, and this work can be continued. Future work should include some changes, including staining with a B4GALT1 antibody during confocal microscopy to confirm if the number of tagged B4GALT1 enzymes is one in six as calculated from the western blot analysis, as well as to confidently see if B4GALT1HaloTag is localising to the same place as endogenous B4GALT1.

## The Quantification of the TIRFM Evanescent Field

TIRF microscopy is an excellent tool for the visualisation and investigation of single fluorophores in real time in 3D. TIRF microscopy's high signal to noise ratio allows for high sensitivity to changes in fluorescence which correlate to movement of fluorophores in the z-direction, a feature which has been used in multiple past assays to investigate vesicles (Viet *et al.,* 2022, Nikolaus *et al*., 2012). However, there are several challenges associated with the calibration of TIRFM, one of which include multiple conflicting methods to determine the depth of the evanescent field and therefore quantify the movement of particles in the z-direction, as discussed in Chapter 1. As part of the development of the tools required for visualising intra-Golgi vesicle trafficking, this project aimed to develop a

reliable method for determining the depth of the evanescent field, data which can then be extrapolated to future TIRFM experiments and cell free assays. This was achieved through the study of previously tagged and isolated B4GALT1-YFP vesicles.

This study successfully determined the number of YFP molecules in vesicles through comparing their relative fluorescence and generating a histogram from a large data set of the intensity versus area for individual vesicles. This data showed that most vesicles contained 1 YFP (62.61%), followed by 2 YFPs (26.27%), 3 YFPs (7.60%) and 4 or more YFPs (3.52%). From this knowledge, TIRFM was then utilised to successfully generate an intensity versus distance from slide graph. However, the generation of this graph required assumptions, including the size of each vesicle being 50nm in diameter. This presumption is a best guess based on the current literature, however different assays state slightly different ranges of sizes, from 52nm (Mironov *et al*., 2017) to 45-50nm (Beznoussenko *et al*., 2016). However other articles describe COPI vesicles to be larger, from 60-90nm (Bonfanti *et al.*, 1998) to 70-80nm (Orci *et al*., 1986). Future work to confirm the size of the B4GALT1-YFP vesicles would be required to improve the accuracy of the intensity versus distance from slide graph, such as DLS or electron microscopy.

Despite these assumptions, this study successfully generated an intensity versus distance from slide graph for future reference in order to estimate the movement of a fluorophore in the z-direction from its changes in intensity. This graph determined the maximum distance from the slide that YFP is sufficiently excited is 99.52nm, which is a more accurate representation of the depth of the evanescent wave compared to using known equations to calculate the theoretical depth of the evanescent field which have previously been shown to be flawed (Brunstein *et al.,* 2014). This is reflected in the use of Equation 1 to calculate the depth of the evanescent field, which produced a value of 68.17nm as the depth of the evanescent field. These equations should be taken as first approximations to the depth of the evanescent field, and scattering causes deviations from the theoretical calculated depths (Axelrod and Axelrod, 2021).

The adhesion of the vesicles on the poly-lysine slides was confirmed through the plotting of each vesicle's minimum and maximum intensity onto a scatter graph. This data shows that on average the vesicles on the poly-lysine coated slides have higher minimum and maximum intensities than the vesicles on uncoated slides, something which is expected for vesicles stuck on the surface of the slide and therefore fluoresce brighter. However, these results also show that the vesicles on the poly-lysine coated slides have a higher range between the highest and lowest recorded intensities compared to the vesicles on the uncoated slides, indicating that they have a larger range of movement in the z-direction. This is unexpected as poly-lysine is known to strongly adhere vesicles to glass slides,

therefore limiting their movement in the z-direction (Stil *et al.,* 2023). Furthermore, the minimum and maximum intensities for the surface-immobilised vesicles are overall higher, which is most likely caused by a higher fluorescence background due to surface impurities introduced during the poly-lysine surface coating step. This can be mitigated through taking extra care in cleaning the glass slides and filtering the poly-lysine solution before applying to slides, however this only minimises impurities and most likely similar results will be seen in future studies.

In future assays, the B4GALT1-HaloTag and MGAT1-SNAPTag transfected cells could be visualised with TIRFM, using HaloTag and SNAPTag ligand fluorophores. These fluorophores may show a different brightness or ranges within the evanescent field that they can be sufficiently excited, meaning that the intensity versus distance from slide graph would need to be adjusted. The method for doing so can be repeated from the method described in this study. The use of these new fluorophores will however be an advantage to a cell free assay, as their higher photostability compared to YFP will allow for the investigation of vesicle approach to the cisternae in greater detail, overcoming issues encountered with YFP in the past (Fisher *et al.,* 2019, Cottam *et al*., 2014).

## Future Potential

The aim of this project was to prepare the tools required for the TIRFM analysis of intra-Golgi vesicles. This has been achieved through the generation and validation of plasmids expressing B4GALT1-HaloTag and MGAT1-SNAPTag, as well as establishing a method for the determination of the number of fluorescently tagged proteins in vesicles, and the quantification of a fluorophore's intensity in relation to its distance from the slide surface in TIRF microscopy. This work can be continued in the future to investigate the mechanisms behind intra-Golgi vesicle trafficking, tethering and fusion, which can be achieved through the isolation of the Golgi cisternae and vesicles, staining with differing HaloTag and SNAPTag ligands, adhering the Golgi cisternae to a poly-lysine coated slide, and then introducing differently stained vesicles and visualise their adhesion and fusion with the Golgi cisternae with TIRFM (Figure 25).

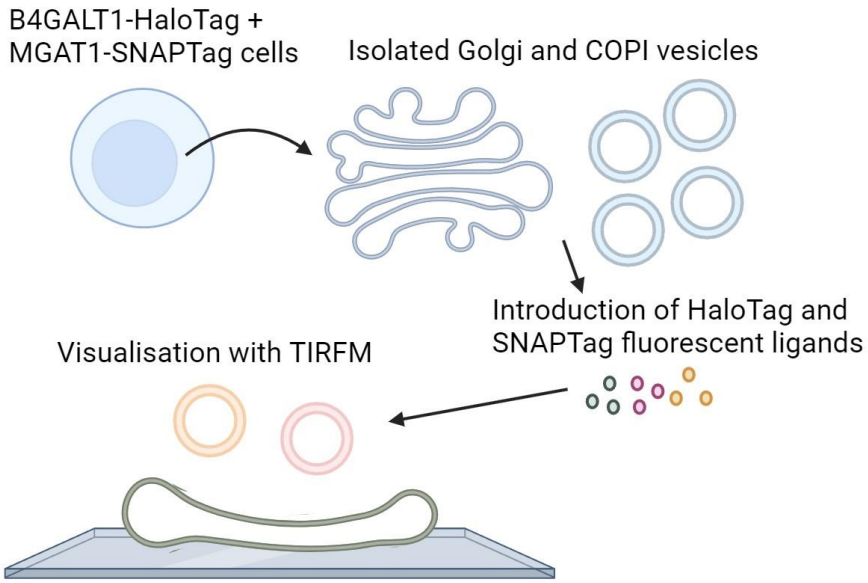


***Figure 25*** **- Schematic figure of future work with B4GALT1-HaloTag + MGAT1-SNAPTag cells.**

There is a lot of potential with this type of assay, as the effects of the introduction of inhibitors to known tethering factors or CRISPR/Cas9 point mutations can be visualised. The study of mutations to understand the roles of tethering factors within the Golgi is something that has extensively been studied in the past (Cottam *et al.,* 2014, Willett *et al*., 2013 Park *et al.*, 2022), however those studies were not able to visualise how the mutations affected the movement of vesicles in real time, as well as the sequence of interactions and their timings, something that this assay has the potential to reveal.

## Concluding Remarks

The work from this study has the potential to uncover vital information about vesicle tethering and fusion within the Golgi apparatus, a process which is vital in the movement of glycosylation enzymes between the Golgi cisternae to maintain Golgi homeostasis and therefore ensure the correct modification of nascent proteins from the ER. Past research has uncovered a lot of information on the proteins mediating intra-Golgi vesicle trafficking, however limitations in yeast two hybrid and CoImmunoprecipitation assays may not reflect in vivo functionalities, and the lack of real time microscopy has limited the information acquired about the timings of these interactions. Understanding how intra-Golgi vesicle tethering and fusion works is vital in our understanding of cellular function, as well as aiding in the development of effective drugs and therapies that target the secretory pathway, and the understanding of glycosylation defect diseases such as CDGS.

## Supplementary Material

| Video File Number | Upper Threshold | Lower Threshold |
|---|---|---|
| **220811_15x_dil_300mgain_33ms_YFP_1** | 24 | 255 |
| **220811_15x_dil_300mgain_33ms_YFP_2** | 43 | 255 |
| **220811_15x_dil_300mgain_33ms_YFP_3** | 35 | 255 |
| **220811_15x_dil_300mgain_33ms_YFP_4** | 36 | 255 |
| **220811_15x_dil_300mgain_33ms_YFP_5** | 18 | 255 |
| **220811_15x_dil_300mgain_33ms_YFP_6** | 23 | 255 |
| **220811_15x_dil_300mgain_33ms_YFP_7** | 43 | 255 |
| **220811_15x_dil_300mgain_33ms_YFP_8** | 58 | 255 |
| **220811_15x_dil_300mgain_33ms_YFP_9** | 40 | 255 |
| **220811_15x_dil_300mgain_33ms_YFP_10** | 23 | 255 |
| **220811_15x_dil_300mgain_33ms_YFP_11** | 21 | 255 |
| **220811_15x_dil_300mgain_33ms_YFP_12** | 46 | 255 |
| **220811_15x_dil_300mgain_33ms_YFP_13** | 20 | 255 |
| **220811_15x_dil_300mgain_33ms_YFP_14** | 35 | 255 |
| **220811_15x_dil_300mgain_33ms_YFP_15** | 26 | 255 |
| **220811_15x_dil_300mgain_33ms_FM143_1** | 44 | 255 |
| **220811_15x_dil_300mgain_33ms_FM143_2** | 58 | 255 |
| **220811_15x_dil_300mgain_33ms_FM143_3** | 24 | 255 |
| **220811_15x_dil_300mgain_33ms_FM143_4** | 52 | 255 |
| **220811_15x_dil_300mgain_33ms_FM143_5** | 26 | 255 |
| **220811_15x_dil_300mgain_33ms_FM143_6** | 43 | 255 |
| **220811_15x_dil_300mgain_33ms_FM143_7** | 41 | 255 |
| **220811_15x_dil_300mgain_33ms_FM143_8** | 18 | 255 |
| **220811_15x_dil_300mgain_33ms_FM143_9** | 14 | 255 |

| | | |
|---|---|---|
| **220811_15x_dil_300mgain_33ms_FM143_10** | 24 | 255 |
| **220811_15x_dil_300mgain_33ms_FM143_11** | 41 | 255 |
| **220811_15x_dil_300mgain_33ms_FM143_12** | 35 | 255 |
| **220811_15x_dil_300mgain_33ms_FM143_13** | 32 | 255 |
| **220811_15x_dil_300mgain_33ms_FM143_14** | 44 | 255 |
| **220811_15x_dil_300mgain_33ms_FM143_15** | 30 | 255 |

***Supplementary Table 1 – Upper and lower background threshold for ImageJ analysis of TIRFM videos.***

| **Video File Number** | **Area Range of Vesicles Selected** | **Y Intercept** | **$R^2$** |
|---|---|---|---|
| **220811_15x_dil_300mgain_33ms_YFP_1** | 0 – 0.80 | 48.263 | 0.709 |
| **220811_15x_dil_300mgain_33ms_YFP_2** | 0 – 0.60 | 62.737 | 0.715 |
| **220811_15x_dil_300mgain_33ms_YFP_3** | 0 – 1.50 | 27.465 | 0.649 |
| **220811_15x_dil_300mgain_33ms_YFP_4** | 0 – 0.80 | 55.278 | 0.752 |
| **220811_15x_dil_300mgain_33ms_YFP_5** | 0 – 1.20 | 50.227 | 0.676 |
| **220811_15x_dil_300mgain_33ms_YFP_6** | 0 – 1.20 | 41.544 | 0.681 |
| **220811_15x_dil_300mgain_33ms_YFP_7** | 0 – 0.95 | 48.203 | 0.658 |
| **220811_15x_dil_300mgain_33ms_YFP_8** | 0 – 0.50 | 43.237 | 0.614 |
| **220811_15x_dil_300mgain_33ms_YFP_9** | 0 – 1.00 | 19.414 | 0.797 |
| **220811_15x_dil_300mgain_33ms_YFP_10** | 0 – 0.50 | 12.201 | 0.806 |
| **220811_15x_dil_300mgain_33ms_YFP_11** | 0 – 1.00 | 25.062 | 0.848 |
| **220811_15x_dil_300mgain_33ms_YFP_12** | 0 – 0.80 | 47.466 | 0.753 |
| **220811_15x_dil_300mgain_33ms_YFP_13** | 0 – 0.60 | 34.820 | 0.834 |
| **220811_15x_dil_300mgain_33ms_YFP_14** | 0 – 0.80 | 49.322 | 0.816 |
| **220811_15x_dil_300mgain_33ms_YFP_15** | 0 – 0.80 | 31.859 | 0.867 |
| **220811_15x_dil_300mgain_33ms_FM143_1** | All | 23.412 | 0.718 |

| | | | |
|---|---|---|---|
| **220811_15x_dil_300mgain_33ms_FM143_2** | All | 42.419 | 0.834 |
| **220811_15x_dil_300mgain_33ms_FM143_3** | All | 31.276 | 0.813 |
| **220811_15x_dil_300mgain_33ms_FM143_4** | 0 – 0.06 | 36.465 | 0.727 |
| **220811_15x_dil_300mgain_33ms_FM143_5** | 0 – 0.25 | 16.883 | 0.817 |
| **220811_15x_dil_300mgain_33ms_FM143_6** | All | 24.016 | 0.670 |
| **220811_15x_dil_300mgain_33ms_FM143_7** | All | 53.966 | 0.445 |
| **220811_15x_dil_300mgain_33ms_FM143_8** | 0 – 0.5 | 55.789 | 0.788 |
| **220811_15x_dil_300mgain_33ms_FM143_9** | All | 36.503 | 0.867 |
| **220811_15x_dil_300mgain_33ms_FM143_10** | 0 – 0.26 | 21.870 | 0.759 |
| **220811_15x_dil_300mgain_33ms_FM143_11** | 0 – 0.25 | 16.318 | 0.728 |
| **220811_15x_dil_300mgain_33ms_FM143_12** | All | 50.609 | 0.862 |
| **220811_15x_dil_300mgain_33ms_FM143_13** | All | 10.249 | 0.819 |
| **220811_15x_dil_300mgain_33ms_FM143_14** | All | 32.661 | 0.728 |
| **220811_15x_dil_300mgain_33ms_FM143_15** | 0 – 0.30 | 18.208 | 0.758 |

***Supplementary Table 2 – Parameters for selection of area/intensities of vesicles, as well as Y intercept and $R^2$ values of scatter graphs created.***

# References

Adolf, F., Herrmann, A., Hellwig, A., Beck, R., Brügger, B. and Wieland, F.T. (2013). "Scission of COPI and COPII Vesicles Is Independent of GTP Hydrolysis." Traffic 14(8): pp.922-932. [Online]. DOI:

10.1111/j.1365-2141.1975.tb01833.x [2 August 2022].

Allan, B. B., Moyer, B.D. and Balch, W.E. (2000). "Rab1 recruitment of p115 into a cis-SNARE complex: programming budding COPII vesicles for fusion." Science 289(5478): pp.444-448. [Online]. DOI: 10.1126/science.289.5478.444 [19 January 2023].

Aryal, C. M., Tyoe, O. and Diao, J. (2021). "Lipid Species Dependent Vesicles Clustering Caused by alpha-Synuclein as Revealed by Single-Vesicle Imaging with Total Internal Reflection Fluorescence Microscopy." Biophys. Rep. 7(6): p.437. [Online]. DOI: 10.52601/bpr.2021.210020 [17 August 2023].

Axelrod, J.J. and Axelrod, D. (2021). “Light scattering in TIRF microscopy: A theoretical study of the limits to surface selectivity.” Biophys. J. 120(15): pp.2952-2968. [Online]. DOI:

10.1016/j.bpj.2021.06.025 [26 September 2023].

Balch, W. E., Dunphy, W.G., Braell, W.A. and Rothman, J.E. (1984). "Reconstitution of the transport of protein between successive compartments of the Golgi measured by the coupled incorporation of N-acetylglucosamine." Cell 39(2): pp.405-416. [Online]. DOI: 10.1016/0092-8674(84)90019-9 [23 August 2022].

Becherer, U., Pasche, M., Nofal, S., Hof, D., Matti, U. and Rettig, J. (2007). "Quantifying Exocytosis by Combination of Membrane Capacitance Measurements and Total Internal Reflection Fluorescence Microscopy in Chromaffin Cells." PloS one 2(6): p.e505. [Online]. DOI:

10.1371/journal.pone.0000505 [25 August 2023].

Beznoussenko, G. V., Ragnini-Wilson, A., Wilson, C. and Mironov, A.A. (2016). "Three-dimensional and immune electron microscopic analysis of the secretory pathway in Saccharomyces cerevisiae." Histochem. Cell Biol. 146: pp.515-527. [Online]. DOI: 10.1007/s00418-016-1483-y [18 February 2023].

Blackburn, J. B., D'Souza, Z. and Lupashin, V.V. (2019). "Maintaining order: COG complex controls Golgi trafficking, processing, and sorting." FEBS letters 593(17): pp.2466-2487. [Online]. DOI:

10.1002/1873-3468.13570 [17 August 2023].

Bonfanti, L., Mironov, A.A., Martínez-Menárguez, J.A., Martella, O., Fusella, A., Baldassarre, M., Buccione, R., Geuze, H.J. and Luini, A. (1998). "Procollagen traverses the Golgi stack without leaving the lumen of cisternae: evidence for cisternal maturation." Cell 95(7): pp.993-1003. [Online]. DOI:

10.1016/s0092-8674(00)81723-7 [25 April 2023].

Brunstein, M., Teremetz, M., Hérault, K., Tourain, C. and Oheim, M. (2014). "Eliminating Unwanted

Far-Field Excitation in Objective-Type TIRF. Part I. Identifying Sources of Nonevanescent Excitation Light." Biophys. J. 106(5): pp.1020-1032. [Online]. DOI: 10.1016/j.bpj.2013.12.051 [3 September 2023].

Cole, N. B., Sciaky N., Marotta A., Song J., Lippincott-Schwartz J. (1996). “Golgi dispersal during microtubule disruption: regeneration of Golgi stacks at peripheral endoplasmic reticulum exit sites.” Mol Biol Cell 7(4): 631-50. [Online]. DOI: 10.1091/mbc.7.4.631 [10 January 2024].

Cottam, N. P., Wilson, K.M., Ng, B.G., Körner, C., Freeze, H.H. and Ungar, D. (2014). "Dissecting functions of the conserved oligomeric Golgi tethering complex using a cell-free assay." Traffic 15(1): pp.12-21. [Online]. DOI: 10.1111/tra.12128 [10 September 2022].

Cottam, N. P. and Ungar, D. (2012). "Retrograde vesicle transport in the Golgi." Protoplasma 49: pp.943-955. [Online]. DOI: 10.1083/jcb.143.3.589 [15 September 2023].

Dulary, E., Potelle, S., Legrand, D. and Foulquier, F. (2017). "TMEM165 deficiencies in Congenital Disorders of Glycosylation type II (CDG-II): Clues and evidences for roles of the protein in Golgi functions and ion homeostasis." Tissue and Cell 49(2): pp.150-156. [Online]. DOI:

10.1016/j.tice.2016.06.006 [27 August 2023].

England, C. G., Luo, H. and Cai, W. (2015). "HaloTag Technology: A Versatile Platform for Biomedical Applications." Bioconjug Chem. 26(6): pp.975-986. [Online]. DOI: 10.1021/acs.bioconjchem.5b00191 [10 September 2023].

Fish, K. N. (2009). "Total Internal Reflection Fluorescence (TIRF) Microscopy." Curr. Protoc. Cytom. 50(1): pp.12-18. [Online]. DOI: 10.1002/0471142956.cy1218s50 [15 September 2022].

Fisher, P., Spencer, H., Thomas-Oates, J., Wood, A.J. and Ungar, D. (2019a). "Modelling Glycan

Processing Reveals Golgi-Enzyme Homeostasis upon Trafficking Defects and Cellular Differentiation." Cell Rep. 27(4): pp.1231-1243. [Online]. DOI: 10.1016/j.celrep.2019.03.107 [4 December 2022].

Fisher, P., Thomas-Oates, J., Wood, A.J. and Ungar, D. (2019b). "The N-glycosylation processing potential of the mammalian Golgi apparatus." Front. Cell Dev. Biol. 7: p.157. [Online]. DOI:

10.3389/fcell.2019.00157 [13 September 2022].

Foulquier, F., Vasile, E., Schollen, E., Callewaert, N., Raemaekers, T., Quelhas, D., Jaeken, J., Mills, P., Winchester, B., Krieger, M. and Annaert, W. (2006). "Conserved oligomeric Golgi complex subunit 1 deficiency reveals a previously uncharacterized congenital disorder of glycosylation type II." PNAS 103(10): pp.3764-3769. [Online]. DOI: 10.1073/pnas.0507685103 [6 September 2023].

Freedman, D. and Diaconis, P. (1981). "On the histogram as a density estimator:L2 theory." Zeitschrift für Wahrscheinlichkeitstheorie und verwandte Gebiete 57(4): pp.453-476. [Online]. DOI:

10.1007/bf01025868 [9 August 2023].

Ghosh, S. K. (2020). "Camillo Golgi (1843 –1926): scientist extraordinaire and pioneer figure of modern neurology."Anat Cell Biol. 53(4): pp.385-392. [Online]. DOI: 10.5115/acb.20.196 [22 April 2023].

Gremillion, S. K., Harris, S.D., Jackson-Hayes, L., Kaminskyj, S.G.W., Loprete, D.M., Gauthier, A.C.,

Mercer, S., Ravita, A.J. and Hill, T.W. (2014). "Mutations in proteins of the Conserved Oligomeric

Golgi Complex affect polarity, cell wall structure, and glycosylation in the filamentous fungus Aspergillus nidulans." Fungal Genet. Biol.73: pp.69-82. [Online]. DOI: 10.1016/j.fgb.2014.10.005 [16 April 2023].

Happe, S. and Weidman, P. (1998). "Cell-free Transport to Distinct Golgi Cisternae Is Compartment Specific and ARF Independent." JCB. 140(3): pp.511-523. [Online]. DOI: 10.1083/jcb.140.3.511 [19 July 2023].

Honda, A., Al-Awar, O.S., Hay, J.C. and Donaldson, J.G. (2005). "Targeting of Arf-1 to the early Golgi by membrin, an ER-Golgi SNARE." JCB. 168(7): pp.1039-1051. [Online]. DOI: 10.1083/jcb.200409138 [9 August 2023].

Jamieson, J. D. and Palade, G.E. (1967). "Intracellular transport of secretory proteins in the pancreatic exocrine cell: I. Role of the peripheral elements of the Golgi complex." JCB. 34(2): pp.577596. [Online]. DOI: 10.3389 [25 August 2023].

Klumperman, J. (2011). "Architecture of the Mammalian Golgi." Cold Spring Harb. perspect. biol. 3(7): p.a005181. [Online]. DOI: 10.1101/cshperspect.a005181 [16 April 2023].

Koumandou, V. L., Dacks, J.B., Coulson, R.M. and Field, M.C. (2007). "Control systems for membrane fusion in the ancestral eukaryote; evolution of tethering complexes and SM proteins." BMC Elol. Biol. 7: pp.1-17. [Online]. DOI: 10.1186/1471-2148-7-29 [25 September 2023].

Kudalkar, E. M., Davis, T.N. and Asbury, C.L. (2016). "Single-Molecule Total Internal Reflection Fluorescence Microscopy." Cold Spring Harb. Protoc. 2016(5): pp.pdb-top077800. [Online]. DOI:

10.1101/pdb.top077800 [5 August 2023].

Laufman, O., Hong, W. and Lev, S. (2013). "The COG complex interacts with multiple Golgi SNAREs and enhances fusogenic assembly of SNARE complexes." J. Cell Sci. 126(6): pp.1506-1516. [Online]. DOI: 10.1242/jcs.122101 [29 August 2023].

Li, J., Ahat, E. and Wang, Y. (2019). "Golgi Structure and Function in Health, Stress, and Diseases." The Golgi Apparatus and Centriole: Functions, Interactions and Role in Disease: pp.441-485. [Online]. DOI: 10.1007/978-3-030-23173-6_19 [22 July 2023].

Locatelli-Hoops, S., Sheen, F. C., Lioudmila, Z., Gawrisch, K. and Yeliseev, A. A. (2013). “Application of HaloTag Technology to Expression and Purification of Cannabinoid Receptor CB2.” Protein Expr Purif. 89(1): 62–72. [Online]. DOI: 10.1016/j.pep.2013.02.011 [11 Jan 2024].

Malsam, J., Satoh, A., Pelletier, L. and Warren, G. (2005). "Golgin Tethers Define Subpopulations of COPI Vesicles." Science 307(5712): pp.1095-1098. [Online]. DOI: 10.1126/science.1108061 [25 September 2023].

Martin-Fernandez, M. L., Tynan, C.J. and Webb, S.E.D. (2013). "A ‘pocket guide’ to total internal reflection fluorescence." J. Microsc. 252(1): pp.16-22. [Online]. DOI: 10.1111/jmi.12070 [25 August 2023].

Miller, V. J., Sharma, P., Kudlyk, T.A., Frost, L., Rofe, A.P., Watson, I.J., Duden, R., Lowe, M., Lupashin, V.V. and Ungar, D. (2013). "Molecular insights into vesicle tethering at the Golgi by the conserved

oligomeric Golgi (COG) complex and the golgin TATA element modulatory factor (TMF)." JBC 288(6): pp.4229-4240. [Online]. DOI: 10.1074/jbc.M112.426767 [12 August 2022].

Mironov, A.A., Sesorova, I.S., Seliverstova, E.V. and Beznoussenko, G.V. (2017). “Different Golgi ultrastructure across species and tissues: Implications under functional and pathological conditions, and an attempt at classification.” Tissue and Cell 49(2): pp.186-201. [Online]. DOI:

10.1016/j.tice.2016.12.002 [28 September 2023].

Mkhikian, H., Mortales, C.L., Zhou, R.W., Khachikyan, K., Wu, G., Haslam, S.M., Kavarian, P., Dell, A. and Demetriou, M. (2016). "Golgi self-correction generates bioequivalent glycans to preserve cellular homeostasis." Elife 5: p.e14814. [Online]. DOI: 10.7554/eLife.14814 [28 July 2023].

New England Biolabs (2022). High Efficiency Transformation Protocol (C2987H) V.3. [Online]. New England Biolabs (NEB), UK. https://www.protocols.io/view/high-efficiency-transformation-protocolc2987h-95qpvoqxl4o1/v3 [29 July 2022].

New England Biolabs (2023). Restriction Endonucleases. [Online]. New England Biolabs (NEB), UK. https://www.neb.com/en-gb/products/restriction-endonucleases [8 July 2022].

Nikolaus, J., Hancock, K., Tsemperouli, M., Baddeley, D. and Karatekin, E. (2021). "Optimal Detection of Fusion Pore Dynamics Using Polarized Total Internal Reflection Fluorescence Microscopy." Front. Mol. Biosci. 8: p.740408. [Online]. DOI: 10.3389/fmolb.2021.740408 [9 November 2022].

Orci, L., Glick, B.S. and Rothman, J.E. (1986). “A new type of coated vesicular carrier that appears not to contain clathrin: its possible role in protein transport within the Golgi stack.” Cell, 46(2): pp.171184. [Online]. DOI: 10.1016/j.tice.2016.12.002 [28 September 2023].

Park, S. Y., Muschalik, N., Chadwick, J. and Munro, S. (2022). "In vivo characterization of Drosophila golgins reveals redundancy and plasticity of vesicle capture at the Golgi apparatus." Curr. Biology 32(21): pp.4549-4564. [Online]. DOI: 10.1016/j.cub.2022.08.054 [28 July 2023].

Popoff, V., Adolf, F., Brügger, B. and Wieland, F. (2011). "COPI Budding within the Golgi Stack." Cold Spring Harb. perspect. biol. 3(11): p.a005231. [Online]. DOI: 10.1101/cshperspect.a005231 [3 May 2023].

Promega (2010). Wizard® Plus SV Minipreps DNA Purification System. [Online]. Promega, USA. https://www.promega.co.uk/-/media/files/resources/protocols/technical-bulletins/0/wizard-plussv-minipreps-dna-purification-systemprotocol.pdf?rev=ef93f7f0a2e142c68e9d6daff234ae8b&sc_lang=en [5 August 2023].

Promega (2023). PureYield™ Plasmid Midiprep System. [Online]. Promega, USA.

https://www.promega.co.uk/-/media/files/resources/protocols/technical-manuals/0/pureyieldplasmid-midiprep-system-protocol.pdf?rev=0dac7547c4b147f9931824e57e7a91ac&sc_lang=en [10 August 2023].

Qasba, P. K., Ramakrishnan, B. and Boeggeman, E (2008). "Structure and function of β-1, 4galactosyltransferase." Curr. Drug Targets 9(4): pp.292-309. [Online]. DOI:

10.2174/138945008783954943 [29 August 2023].

Reinhard, C., Schweikert, M., Wieland, F.T. and Nickel, W. (2003). "Functional reconstitution of COPI coat assembly and disassembly using chemically defined components." PNAS 100(14): pp.8253-8257.

[Online]. DOI: 10.1073/pnas.1432391100 [14 November 2022].

Schaub, B.E., Berger, B., Berger, E.G. and Rohrer, J., (2006). “Transition of galactosyltransferase 1 from trans-Golgi cisterna to the trans-Golgi network is signal mediated”. MBoC, 17(12), pp.51535162. [Online]. DOI: 10.1073/pnas.1432391100 [28 September 2023].

Schmitz, K. R., Liu, J., Li, S., Setty, T.G., Wood, C.S., Burd, C.G. and Ferguson, K.M. (2008). "Golgi localization of glycosyltransferases requires a Vps74p oligomer." Dev. Cell14(4): pp.523-534.

[Online]. DOI: 10.1016/j.devcel.2008.02.016 [7 January 2023].

Schoberer, J., Liebminger, E., Botchway, S.W., Strasser, R. and Hawes, C. (2013). "Time-Resolved

Fluorescence Imaging Reveals Differential Interactions of N-Glycan Processing Enzymes across the Golgi Stack in Planta." Plant Physiol. 161(4): pp.1737-1754. [Online]. DOI: 10.1104/pp.112.210757 [11 August 2023].

Sørensen, D. M., Büll, C., Madsen, T.D., Lira-Navarrete, E., Clausen, T.M., Clark, A.E., Garretson, A.F., Karlsson, R., Pijnenborg, J.F., Yin, X. and Miller, R.L. (2023). "Identification of global inhibitors of cellular glycosylation." Nat. Commun. 14(1): p.948. [Online]. DOI: 10.1038/s41467-023-36598-7 [3 May 2023].

Stil, A., Liberelle, B., Guadarrama Bello, D., Lacomme, L., Arpin, L., Parent, P., Nanci, A., Dumont, É.C., Ould-Bachir, T., Vanni, M.P. and De Crescenzo, G. (2023). "A simple method for poly-d-lysine coating to enhance adhesion and maturation of primary cortical neuron cultures in vitro." Front. Cell. Neurosci.17: p.1212097. [Online]. DOI: 10.3389/fncel.2023.1212097 [23 August 2022].

Suga, A., Nagae, M. and Yamaguchi, Y. (2018). "Analysis of protein landscapes around Nglycosylation sites from the PDB repository for understanding the structural basis of N-glycoprotein processing and maturation." Glycobiology 28(10): pp.774-785. [Online]. DOI:

10.1093/glycob/cwy059 [28 June 2023].

Tie, H. C., Mahajan, D. and Lu, L. (2022). "Visualizing intra-Golgi localization and transport by sideaveraging Golgi ministacks." JCB 221(6): p.e202109114. [Online]. DOI: 10.1083/jcb.202109114 [25 September 2023].

Ungar, D., Oka, T., Vasile, E., Krieger, M. and Hughson, F.M. (2005). "Subunit architecture of the conserved oligomeric Golgi complex." JBC 280(38): pp.32729-32735. [Online]. DOI:

10.1074/jbc.M504590200 [3 November 2022].

van Bommel, D. M., Toonen, R.F. and Verhage, M. (2023). "Mapping localization of 21 endogenous proteins in the Golgi apparatus of rodent neurons." Sci. Rep. 13(1): p.2871. [Online]. DOI:

10.1038/s41598-023-29998-8 [3 November 2022].

Veit, S., Paweletz, L.C., Bohr, S.S.R., Menon, A.K., Hatzakis, N.S. and Pomorski, T.G. (2022). "Single Vesicle Fluorescence-Bleaching Assay for Multi-Parameter Analysis of Proteoliposomes by Total Internal Reflection Fluorescence Microscopy." ACS 14(26): pp.29659-29667. [Online]. DOI:

10.1021/acsami.2c07454 [3 November 2022].

Walter, D. M., Paul, K.S. and Waters, M.G. (1998). "Purification and characterization of a novel 13 S hetero-oligomeric protein complex that stimulates in Vitro Golgi transport." JBC 273(45): pp.2956529576. [Online]. DOI: 10.1074/jbc.273.45.29565 [15 September 2023].

Weber, S., Hofmann, A., Herms, S., Hoffmann, P. and Doerfler, W. (2015). "Destabilization of the human epigenome: consequences of foreign DNA insertions." Epigenomics 7(5): pp.745-755. [Online]. DOI: 10.2217/epi.15.40 [3 November 2022].

Willett, R., Ungar, D. and Lupashin, V. (2013). "The Golgi puppet master – COG complex at center stage of membrane trafficking interactions." Histochem. Cell Biol. 140: pp.271-283. [Online]. DOI:

10.1007/s00418-013-1117-6 [3 August 2022].

Yadav, A., et al. (2022). "Glycan processing in the Golgi as optimal information coding that constrains cisternal number and enzyme specificity." Elife 11: p.e76757. [Online]. DOI: 10.7554/eLife.76757 [7 August 2022].

Yip, B., Chen, S.H., Mulder, H., Höppener, J.W. and Schachter, H. (1997). "Organization of the human β-1, 2-N-acetylglucosaminyltransferase I gene (MGAT1), which controls complex and hybrid N-glycan synthesis." J. Biochem., 321(1): pp.465-474. [Online]. DOI: 10.1042/bj3210465 [9 November 2022].

Zerial, M. and McBride, H. (2001). "Rab proteins as membrane organizers " Nat. Rev. Mol. Cell Biol. 2(2): pp.107-117. [Online]. DOI: 10.3389 [15 September 2023].